https://doi.org/10.5194/egusphere-2025-6565
Preprint. Discussion started: 30 January 2026

Effect of a Bering Strait Closure on AMOC Resilience in a Climate Box Model

Jelle Soons[1], Elian Vanderborght[1], and Henk A. Dijkstra[1]

[1]Institute for Marine and Atmospheric Research, Utrecht University, Princetonplein 5, 3584 CC Utrecht, The Netherlands

Correspondence: Jelle Soons (j.soons@uu.nl)

Abstract. Recent simulations in an EMIC (CLIMBER-X) have shown that a constructed closure of the Bering Strait can shift the safe carbon budget of the Atlantic Meridional Overturning Circulation (AMOC). In this study we extend a conceptual ocean box model by introducing an atmospheric temperature forcing and a freshwater transport induced by the Bering Strait Throughflow (BST). With this model we can replicate the results produced by CLIMBER-X, and test their sensitivity with respect to forcing and BST parameters. Bifurcation analyses show that a closure of the Bering Strait has a destabilizing effect on an AMOC perturbed by freshwater hosing, but can have a stabilizing effect on an AMOC forced by a polar amplification in atmospheric temperatures – provided the freshwater hosing is limited. A temperature-induced weakening of the AMOC sees a reversal of the BST, which then exports relatively saline waters out of the North Atlantic, and so a closure can have a stabilizing effect. The effectiveness of a closure to prevent a temperature-induced AMOC collapse is sensitively dependent on both the BST parameter values and the rate of the applied forcing. Moreover, the timing of the last preventive closure relies heavily on the forcing rate as well. These conceptual results are important for understanding the feasibility of a Bering Strait closure in order to prevent an AMOC collapse under climate change.

1 Introduction

The Atlantic Meridional Overturning Circulation (AMOC) is of vital importance in regulating the present-day global climate. It transports warm surface waters from the tropics northward with a total northward heat transport of roughly 1.5 PW (Johns et al., 2011) at 26°N, which in turn causes Europe to have a relatively warm climate despite its high latitude. An essential mechanism for this overturning circulation is the water mass transformation in the subpolar North Atlantic, where the relatively warm and saline surface waters are cooled by the atmosphere and increase in density to form the cold and saline North Atlantic Deep Water (NADW). This water mass sinks and returns at greater depth southward forming the lower limb of the AMOC (Frajka-Williams et al., 2019).

The AMOC is considered to be a major tipping system in the present-day climate as under sufficient freshwater or climate forcing it can tip to another stable state in a hard-to-reverse transition (Armstrong McKay et al., 2022). We refer to the current state of the AMOC as an “on-state”, while an other stable state with a weak or non-existent overturning circulation in the Atlantic is referred to as an “off-state” or collapsed state. Throughout the AMOC model hierarchy a stable off-state has been found (Dijkstra, 2024) from simple box models (Stommel, 1961; Cessi, 1994) and ocean-only models (Dijkstra,

https://doi.org/10.5194/egusphere-2025-6565
Preprint. Discussion started: 30 January 2026

2007) to Earth system models of intermediate complexity (EMICs) (Rahmstorf et al., 2005) and modern Earth system models (ESMs) (Van Westen and Dijkstra, 2023). The global climate for such an off-state is dramatically changed with –for example– extreme cold events in Northern Europe and shifting precipitation patterns over the Amazon (Van Westen et al., 2024b; Van Westen and Baatsen, 2025).

The main physical mechanism that can destabilize the AMOC and cause it to collapse to a weaker state is the salt-advection feedback. When the AMOC weakens less salinity is transported northward, which decreases the density of the surface waters in the Nordic Seas and inhibits the deep water formation there, and in turn weakens the AMOC further (Marotzke, 2000). Based on observations of the freshwater transport through the southern boundary of the Atlantic it has been concluded that this feedback mechanism is active in the present-day AMOC (Vanderborght et al., 2025). Moreover, multiple studies have indicated that the AMOC is losing resilience and that the onset of a collapse could occur before the end of the century (Boers, 2021; Ditlevsen and Ditlevsen, 2023; Van Westen et al., 2025b).

Recently it has been shown in the EMIC CLIMBER-X that a constructed closure of the Bering Strait can prevent a collapse of the AMOC for particular freshwater and climate forcing scenarios (Soons and Dijkstra, 2025). More specifically, in this EMIC an AMOC in equilibrium under sufficiently low freshwater hosing sees a larger safe carbon budget when the Strait is closed. This is because for a low enough hosing flux –i.e. a strong enough AMOC– a closure does not only halt the freshwater transport from the Pacific to the Arctic and North Atlantic, but it additionally reduces the freshwater and sea-ice export from the Arctic to the North Atlantic. Hence a closure can have a salinifying effect on the North Atlantic and therefore stabilizes the AMOC. However, for a larger hosing flux –and so a weaker AMOC and fresher North Atlantic– a closure has a freshening effect on the North Atlantic, and hence destabilizes the AMOC. This is due to the fact that for a weaker AMOC the freshwater import through the Bering Strait reduces and now a greatly reduced export of freshwater and sea-ice to the North Atlantic occurs for an open Strait. Therefore there seems to be a critical hosing –and corresponding equilibrium AMOC strength– above (under) which a closure reduces (extends) the AMOC's safe carbon budget.

The overall goal of this paper is to understand the effect of a Bering Strait Dam (BSD) on the tipping behaviour of the AMOC by using a modified version of the conceptual model of Wood et al. (2019). This model is extended by including oceanic temperatures and by representing the effect of the Bering Strait Throughflow (BST) on the AMOC in an idealized setting. This way we can qualitatively reproduce the results found in CLIMBER-X and earlier studies. Moreover, it allows us to assess the sensitivity of the critical hosing level to modeling parameters and type of tipping, i.e. bifurcation- or rate-induced (Ashwin et al., 2012). In section 2 we will introduce the conceptual model and briefly describe CLIMBER-X. In section 3 bifurcation analyses of the new idealized model are performed, accompanied by hysteresis experiments in both models. In section 4 the AMOC is forced with a time-dependent atmospheric temperature increase and subsequently we vary the time of closure of the Strait. Lastly section 5 contains a summary and discussion.

https://doi.org/10.5194/egusphere-2025-6565
Preprint. Discussion started: 30 January 2026

2 Models

2.1 CLIMBER-X configuration

In Soons and Dijkstra (2025) CLIMBER-X was used, which is a fast EMIC allowing for roughly $10,000$ model years per day (Willeit et al., 2022, 2023). It employs the frictional geostrophic 3D ocean model GOLDSTEIN using 23 non-equidistant vertical layers, together with the statistical-dynamical SESAM model for the atmosphere. The sea-ice is modeled using the dynamic-thermodynamic SISIM model, and PALADYN is used for the land surface component. The ice sheets are prescribed at their modern state, and so the net freshwater flux from these sheets is taken to be zero. Furthermore, all components are computed on a horizontal $5° \times 5°$ rectilinear grid. Note that this implies that the Bering Strait lies within a single grid cell. An open Strait is represented by baroclinic tracer exchange between the Arctic and Pacific and is closed for barotropic flow. A closure of the Strait denotes seizing this tracer exchange. Therefore, the BST's strength in this model is unrealistic, while its transport of salinity and heat is captured reasonably well.

Two experiments have been performed in Soons and Dijkstra (2025). Firstly, a hysteresis experiment consisting of a slowly varying hosing flux applied to an equilibrium AMOC for either an open (OBS) or closed Bering Strait (CBS). The hosing with strength F_H was applied to the surface of the Atlantic basin between $20°$N and $50°$N and was surface compensated globally. For both the OBS and CBS hysteresis F_H was initially increased at a rate of 0.025 Sv/kyr till it reaches 0.35 Sv, after which it was decreased with -0.025 Sv/kyr to -0.25 Sv, and finally increased with the initial rate to the pre-industrial level. So each simulation takes $48,000$ yr. The hosing protocol was based on earlier hysteresis experiments in CLIMBER-X (Willeit and Ganopolski, 2024; Boot and Dijkstra, 2025), and show that given these rates the AMOC is in quasi-equilibrium. The second experiment consisted of applying a 1%/yr CO_2 increase to an equilibrium AMOC for various hosing levels F_H under OBS. The initial CO_2 concentration was 280 ppm, and the increase persisted until a prescribed carbon budget is reached. Either the Strait was kept open, or immediately closed at the start of the simulation. For both cases we determined the safe carbon budget (up to 100 PgC accuracy), i.e. the highest possible amount of emissions that can be released at this rate without a collapse. Additionally, in a forcing scenario where an immediate closure prevents a collapse (namely 4900 PgC emissions and no hosing), we delayed the closure in increments of 50 yr to examine the latest closure time that still prevents a collapse.

2.2 A conceptual AMOC model with BST

The conceptual model is based on the ocean model originally introduced by Wood et al. (2019). We will refer to our extended model as the Extended Wood Model (EWM), see Figure 1a. It consists of 5 boxes representing the World Ocean. The northern *N* box corresponds to the North Atlantic Deep Water (NADW) formation region and Arctic region; the *T* box represents the Atlantic thermocline; the *S* box models the fresh Southern Ocean near-surface waters and their return as Antarctic Intermediate Water (AAIW); the *IP* represents the Indo-Pacific thermocline; and the *B* box (bottom box) contains the southward propagating NADW and its upwelling in the Southern Ocean as Circumpolar Deep Water (CDW). The model is calibrated to the stable pre-industrial state of the FAMOUS model (Smith et al., 2008; Smith, 2012), such that it reproduces the decadal means of salinities, temperatures, volumes and transports of this state, and captures the basic physical mechanisms in this more detailed

https://doi.org/10.5194/egusphere-2025-6565
Preprint. Discussion started: 30 January 2026

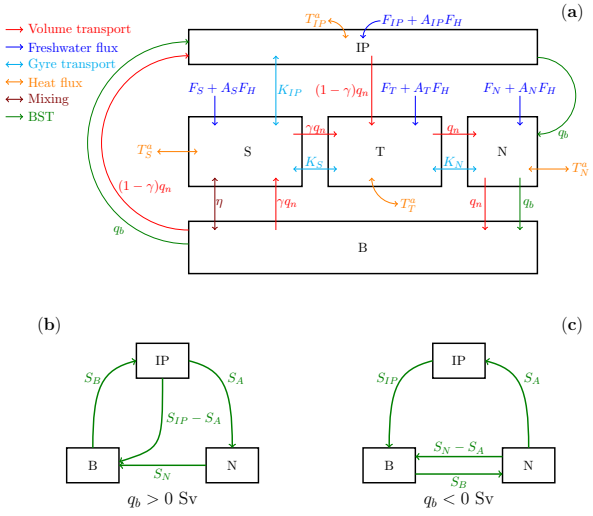

[t]

Figure 1. (**a**) Sketch of the Extended Wood Model (EWM): the red, cyan and blue arrows represent the volume transports between the boxes, the transport by the subtropical gyres, and the freshwater exchange between the ocean's surface and the atmosphere, respectively. The brown and green arrows capture the deep mixing in the Southern Ocean and the BST, respectively, while the orange arrows represent the heat exchange between the ocean's surface and the atmosphere. The boxes' labels are indicated in black. The volume transports induced by an open Bering Strait are depicted with the salinities of these transports added for $q_b > 0$ Sv (**b**) and $q_b < 0$ Sv (**c**).

atmosphere-ocean coupled model. The boxes have salinities denoted by S_N, S_T, S_S, S_{IP} and S_B; temperatures T_N, T_T, T_S, T_{IP} and T_B; and fixed volumes V_N, V_T, V_S, V_{IP} and V_B. Salinity is conserved resulting in a fixed average salinity $\langle S \rangle$.

The following transports occur between the boxes: a downwelling in the North Atlantic (and hence AMOC strength) q_n that acts as a volume transport from the *T* box to the *B* box via the *N* box. A fraction γ of this returns to the *T* box via the Southern Ocean (*S* box) denoted as a cold water path (CWP) , while the remaining fraction $1-\gamma$ returns via a warm water path (WWP) through the Indo-Pacific box. The latter path represents the AMOC return flow via the Agulhas Leakage, while the former models the return flow via the Drake Passage. The strength of this overturning circulation is linearly dependent on the density difference between the northern and southern boxes. As a linear equation of state is assumed, the AMOC strength follows as

$$q_n = \lambda(\alpha(T_S - T_N) - \beta(S_S - S_N)) \tag{1}$$

where λ is a hydraulic constant, α the thermal expansion coefficient, and β the haline contraction coefficient. Moreover, there are gyre transports which are modeled as simple diffusive processes with fixed coefficients K_N, K_S and K_{IP}. The mixing between the Southern Ocean and deep box *B* is captured with the coefficient η. These advective transports –i.e. the volume transports, gyre transports and mixing– transport salinity across the boxes. Additionally, there is a freshwater flux $F_i + C_i F_H$ from the atmosphere into surface box i with $i \in \{N, T, S, IP\}$, where F_i is a fixed atmospheric flux into box i, and C_i the

https://doi.org/10.5194/egusphere-2025-6565
Preprint. Discussion started: 30 January 2026

fraction of the freshwater forcing (i.e. hosing) F_H that goes into box i. Note that in order to conserve salinity we have

$$\sum_{i\in\{N,T,S,IP\}} F_i = 0$$
$$\sum_{i\in\{N,T,S,IP\}} C_i = 0.$$

2.2.1 Model extension with oceanic temperatures

Thus far, the model is identical to the version originally proposed. In that model only temperatures T_S and T_N were relevant, with the former fixed and the latter varying linearly with q_n. We extend it by introducing a complete set of governing equations for the oceanic heat content, in a similar way to the extension proposed of the Cimatoribus et al. (2014) model by Van Westen et al. (2024a). The heat content $V_i T_i$ of box i is altered by either advective transport $\mathcal{F}_i$ from and to other boxes, and –provided box i is a surface box– by an atmospheric heat exchange. This process is modeled with a fixed ocean-atmosphere coupling parameter μ^a, and fixed atmospheric surface temperature T_i^a above surface box i. This yields the set of equations

$$V_i \frac{dT_i}{dt} = \mathcal{F}_i - \mu^a A_i (T_i - T_i^a) \quad \text{for } i \in \{N,T,S,IP\}$$
$$V_B \frac{dT_B}{dt} = \mathcal{F}_B,$$

where A_i is the surface area of surface box i. With the advective transport $\mathcal{F}_i$ we denote the previously described overturning circulation, gyre exchanges and mixing transports. Note that the atmospheric temperatures are fixed, and so the coupling is only from the atmosphere onto the ocean. Therefore an AMOC collapse would not –for example– induce an atmospheric cooling.

These newly introduced heat exchange coefficient, atmospheric temperatures and surface areas need to be determined via a tuning procedure. This procedure is described in more detail in Appendix B. The surface areas are determined using the physical characteristics of the water masses described in Talley (2011). For the heat exchange coefficient we take $\mu^a = 5 \cdot 10^{-6}$m/s, which corresponds to an atmospheric heating of roughly 20 W/(m$^2 \cdot K$) – assuming fixed seawater reference density ρ_0 and heat capacity c_p. The tuning procedure entails finding the atmospheric temperatures such that the equilibrium salinities S_i and oceanic temperatures T_N and T_S are identical to those in the original model version for an active AMOC and no hosing ($q_n > 0$ Sv and $F_H = 0$ Sv). As a simplification we fix that $T_T^a = T_{IP}^a$, and we fix the average atmospheric surface temperature

$$\langle T_a \rangle = \left(\sum_{i\in\{N,T,S,IP\}} A_i T_i^a \right) \Big/ \left(\sum_{i\in\{N,T,S,IP\}} A_i \right).$$

For the analyses presented here we take $\langle T_a \rangle = 14°$C as a pre-industrial value (Inglis et al., 2020). However as a check the tuning is produced for various values of $\langle T_a \rangle$ and μ^a (see Appendix B).

With this extension the model contains a well-known thermal feedback mechanism: a weakening AMOC transports less heat from the tropical box into the northern box, which in turn causes an increase in density ρ_N of the northern box resulting in a strengthening of the AMOC. Hence this a stabilizing feedback, as opposed to the salt-advection feedback. Additionally, this extension allows us to represent the effect of climate change on the AMOC by increasing the northern atmospheric temperature T_N^a in time to mimic polar amplification (Dai, 2022; Soons et al., 2025).

https://doi.org/10.5194/egusphere-2025-6565
Preprint. Discussion started: 30 January 2026

2.2.2 Model extension with BST

The principal new aspect presented in this study is the effect of the BST, labeled q_b. The BST is approximately in geostrophic balance driven by the sea surface height (SSH) difference across the strait, with a lower SSH on the Arctic side. The BST varies linearly with the range of surface buoyancies shared between the Antarctic circumpolar region and the regions of deep water formation in the North Atlantic (Cessi, 2020), and hence we assume for the EWM that $q_b \propto \rho_N - \rho_S$, which is equivalent to simply $q_b \propto q_n$. Moreover, following more-detailed model simulations, for a weakened AMOC the SSH on the Arctic increases (Van Westen et al., 2025a) and causes the reversal of the Throughflow to a net southward flow. Then the freshening effect of the BST on the Northern Atlantic changes to a salinifying effect for a weak enough AMOC strength (De Boer and Nof, 2004; Hu and Meehl, 2005; Hu et al., 2012, 2023), as it now allows for a freshwater transport from the North Atlantic back to the Pacific. This implies that for a sufficiently weak AMOC an open Strait has a stabilizing effect. These previous results are in agreement with the quasi-equilibrium simulations performed in CLIMBER-X (Soons and Dijkstra, 2025). Hence, we model the BST in the EWM as

$$q_b = \nu(q_n - q_0), \tag{2}$$

where $\nu \geq 0$ is a dimensionless hydraulic constant controlling the sensitivity of the BST to variations in q_n, and $q_0 \geq 0$ Sv is the AMOC strength at which the BST transport switches direction.

The transport by the Throughflow consists mainly of relatively fresh Pacific waters, which eventually end up in the deep water formation regions in the North Atlantic where they join the lower limb of the AMOC (Yang and Cessi, 2024). Moreover, an open Strait causes an enhanced freshwater transport from the Arctic to the North Atlantic (Hu et al., 2012; Soons and Dijkstra, 2025). Therefore, the effect of a northward BST ($q_b > 0$ Sv) is modeled as a salinity transport from the Indo-Pacific box *IP* via the northern box *N* to the deep box *B*, from which it returns to box *IP* again. To include the enhanced freshwater exchange with the Arctic we assume that the transport from the *IP* box to the northern box has a fixed Arctic salinity $S_A = 30$ psu (Talley, 2011). The remaining salinity transport $q_b(S_{IP} - S_A)$ joins the AMOC's lower limb in the *B* box. Varying the fixed Arctic salinity with $S_A \in [28, 32]$ psu affects the results only quantitatively. We assume this circulation reverses for $q_b < 0$ Sv, analogous to the circulation driven by the meridional density difference, see Figure 1b-c. The complete model equations and an overview of the adopted parameter values can be found in Appendix A and Appendix C, respectively. Note that we have omitted the heat transport by the BST, since that does not have a large impact on the surface density of the North Atlantic in the EMIC.

Next, the newly introduced parameters ν and q_0 need to be determined. For a closure we simply take $\nu_{CBS} = 0$. Initially, for ν_{OBS} and q_0 we take a range of values in order to examine the AMOC's stability under OBS in the EWM. It was found in more-detailed models that a closure increases the present-day AMOC strength with $(15 \pm 5)\%$ (Hasumi, 2002; Hu et al., 2015). Therefore, for a $q_0 \in [0, 12.5]$ Sv we determine values ν_{10}, ν_{15} and ν_{20} for the OBS setting such that a closure increases the no-hosing equilibrium AMOC strength by respectively 10%, 15% and 20%. The advantage of this tuning procedure is that the additional effects of the BST on the Arctic-Atlantic freshwater exchange –which in turn affects the salinity in the deep-water formation regions– are now aggregated in the transport q_b. Additionally, we perform another tuning of ν and q_0 to CLIMBER-X. In the EMIC a closure increases the AMOC strength by only 2% under pre-industrial conditions, and hence

https://doi.org/10.5194/egusphere-2025-6565
Preprint. Discussion started: 30 January 2026

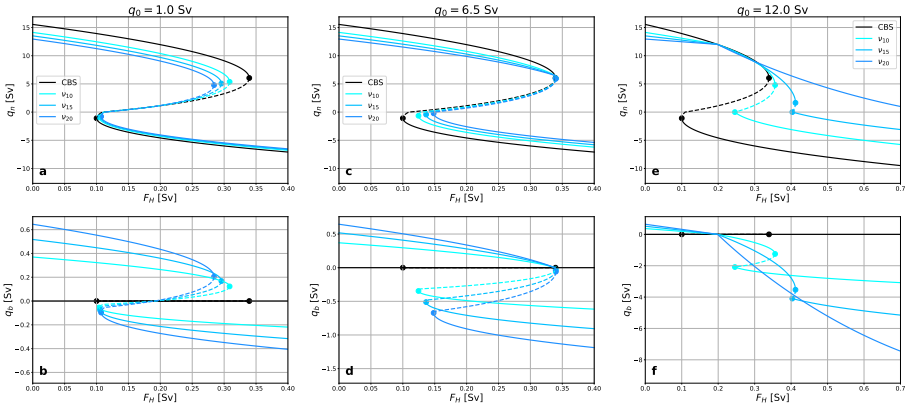

[t]

Figure 2. The bifurcation diagram of the EWM for varying freshwater hosing strength F_H for the AMOC strength q_n (top row) and corresponding BST freshwater transport q_b (bottom row) for either CBS (black), or OBS with parameters ν_{10}, ν_{15} or ν_{20} for increasing shade of blue with corresponding switching AMOC strength q_0 being 1.0 Sv, 6.5 Sv or 12.0 Sv (left to right column), see table D1. Linearly stable branches (solid) and unstable branches (dashed) are connected by saddle-node bifurcations (dots).

$\nu = \nu_2$. Furthermore, in the hysteresis experiment the difference between AMOC strengths under OBS and CBS conditions is negligible after the pre-industrial AMOC strength has reduced by roughly 6.9% to 18.5 Sv. Subsequently, we tune q_0 such that it corresponds to the same proportional reduction, yielding $q_0 = 14.25$ Sv. Since the increase of only 2% falls well below the previous established range we also consider values $\nu_3 (\approx 1.7\nu_2)$ and $\nu_4 (\approx 2.8\nu_2)$ in this case. All BST parameter values can be found in Appendix D.

3 Steady states

3.1 Steady states under varying hosing

We compute bifurcation diagrams of the EWM for varying freshwater hosing strength F_H for CBS and OBS conditions, where we use the parameters in table D1, see Figure 2. The diagram under CBS is qualitatively similar to the earlier result by Alkhayuon et al. (2019) for the original model: a branch of stable AMOC ON states ($q_n > 0$) that eventually ends in a saddle-node bifurcation under sufficiently high freshwater forcing, and a branch of stable AMOC OFF states ($q_n < 0$) that ends via a saddle-node bifurcation for sufficiently low freshwater forcing. There is a regime of freshwater forcings for which both stable states exist, in addition to an unstable state. Two observations can be made considering the addition of the BST. Firstly, if the BST reverses at a sufficiently low enough AMOC strength q_0, an open Strait sees a lower tipping value F_H^1 of the AMOC for freshwater forcing than for a closed Strait, while the reverse is true for a higher q_0. This follows directly from the sign of the transport q_b: if this transport reverses before the AMOC ON state collapses than an open Strait has a salinifying effect on the northern box, and hence it stabilizes the AMOC and extends its tipping point. This is because for $q_b > 0$ Sv the BST replaces North Atlantic water with fresher Arctic water (i.e. $S_N > S_A$), while for $q_b < 0$ Sv it replaces North Atlantic water with more

https://doi.org/10.5194/egusphere-2025-6565
Preprint. Discussion started: 30 January 2026

saline bottom water (i.e. $S_N < S_B$). For $q_0 = 1.0$ Sv an open Strait always has a freshening effect on the *N* box for an AMOC ON state, and so it decreases the critical hosing strength, see Figures 2a-b, while for $q_0 = 12.0$ Sv, an open Strait salinifies the *N* box for $q_n < 12$ Sv and so it extends this critical strength, see Figures 2e-f. Secondly, during an AMOC OFF state an open Strait always has a salinifying effect (since $q_0 \geq 0$ Sv) and therefore the hosing strength F_H^2 at which an OFF state recovers increases, i.e. the AMOC OFF state is destabilized by an open Strait. These shifts in critical hosing values combined yield that for sufficiently high q_0 the hysteresis width decreases substantially under OBS, or even vanishes, as we can see in Figures 2e-f. Here the AMOC's multi-stable regime almost disappears for $\nu = \nu_{15}$ and $q_0 = 12.0$ Sv, and completely disappears for $\nu = \nu_{20}$. The reversed freshwater transport through the open Strait partly supplements the salinity loss of the northern box induced by the AMOC weakening. This prevents the onset of the salt-advection feedback which causes the AMOC's multi-stability. Also, note that for a high switching strength q_0 the AMOC strengths for both OBS and CBS lie quite closely together after the BST has reversed for a range of hosing values. This occurs because the bottom box's salinity and S_N do not differ substantially in this range.

A more thorough analysis of the critical hosing strengths F_H^1 above which the AMOC ON state disappears and F_H^2 below which the AMOC OFF state disappears, and the corresponding hysteresis width $\Delta F_H = F_H^1 - F_H^2$ for the complete range of q_0 is shown in Figure 3. For $q_0 > 5.8$ Sv an open Strait delays the AMOC's freshwater tipping point, while the reverse holds for lower values of q_0. This is because at $q_0 = 5.8$ Sv the BST switches at the tipping point, since $q_n\big|_{F_H^1} = 5.8$ Sv then as well. Hence an open Strait has for a switching strength q_0 around this value neither a salinifying nor freshening effect at the tipping point, and so the critical hosing strength is not altered by it. Note that up to $q_0 \approx 9$ Sv F_H^1 only slightly increases under an open Strait, since for these values the reversed circulation at the tipping point replaces the North Atlantic surface waters of salinity S_N by bottom water of roughly equal salinity S_B. Hence this affects the AMOC's tipping point only marginally. Note also that the BST is salinifying an AMOC OFF state for all $q_0 \geq 0$ Sv, and so F_H^2 increases. The net result of both shifts is that an open Strait causes a decrease in hysteresis width for all $q_0 \geq 0$ Sv with respect to a closed Strait, with multi-stability even vanishing for a large enough switching strength q_0. In this parameter range a hysteresis experiment would not find a multi-stable regime under OBS, but would under CBS, as was seen by Hu et al. (2012) in the CCSM3 model.

We can now also reproduce the hysteresis experiment performed in Soons and Dijkstra (2025) with the conceptual EWM. We increase (and decrease) the hosing strength at the same rate of $dF_H/dt = \pm 0,025$ Sv/kyr under CBS and OBS setting in the EWM. We set the BST parameters to the values derived by the tuning to the EMIC: $q_0 = 14.25$ Sv and vary $\nu \in \{\nu_2, \nu_3, \nu_4\}$. The results are in Figure 4, showing that the simple model for ν_2 can indeed qualitatively reproduce the behaviour of the EMIC, in particular the altered tipping points and increased hysteresis width due to a closure. The same behaviour can also be seen for ν_3 and ν_4, but here with a larger increase for both tipping points. In particular F_H^2 under ν_4 now exceeds F_H^1 under CBS, which is far from the case in CLIMBER-X. Note also that both models show a large overshoot after the AMOC has recovered, since suddenly a large amount of salinity from the Atlantic thermocline is moved northward as the AMOC switches on.

https://doi.org/10.5194/egusphere-2025-6565
Preprint. Discussion started: 30 January 2026

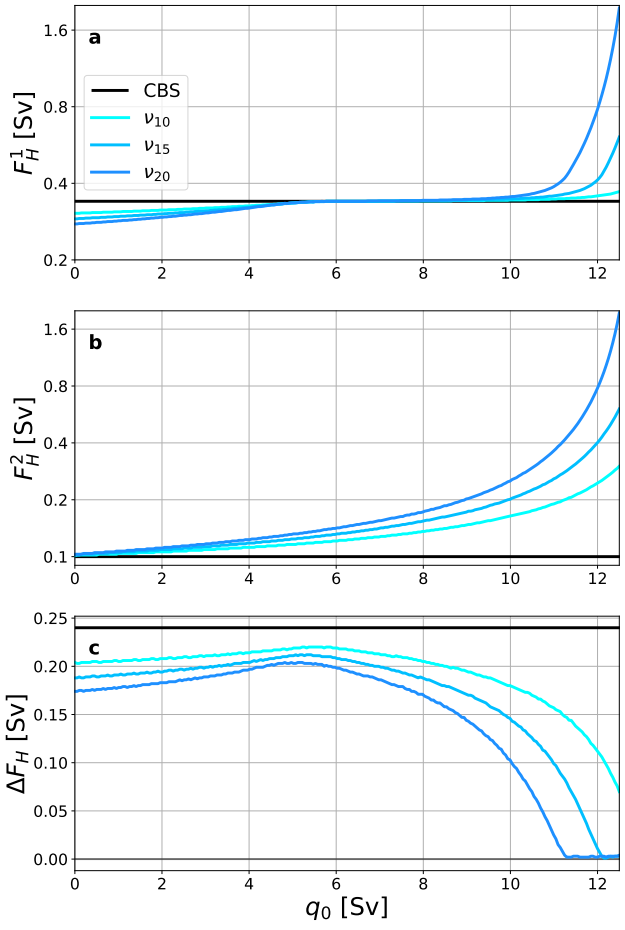

[t]

Figure 3. The critical hosing values F_H^1 (**a**) above which the AMOC ON state disappears, and F_H^2 (**b**) below which the AMOC OFF state disappears, and the corresponding hysteresis width $\Delta F_H = F_H^1 - F_H^2$ (**c**) for a range of $q_0 \in [0, 12.5]$ Sv with corresponding hydraulic constants ν_{10}, ν_{15} or ν_{20} for increasing shade of blue. Note the logarithmic scaling of the top two plots.

3.2 Steady states under Arctic amplification

Next the steady states of the EWM are computed for an Arctic amplification by increasing the northern atmospheric temperature by an amount ΔT_N^a, in order to mimic the destabilizing effect of climate change on the AMOC. So we write from now on $T_N^a = T_N^{a,0} + \Delta T_N^a$, where $T_N^{a,0} = -3.6924°\text{C}$ is our pre-industrial temperature (see also Table C1). Several bifurcation diagrams with increasing Arctic amplification are produced for various fixed hosing strengths under a fixed switching AMOC

https://doi.org/10.5194/egusphere-2025-6565
Preprint. Discussion started: 30 January 2026

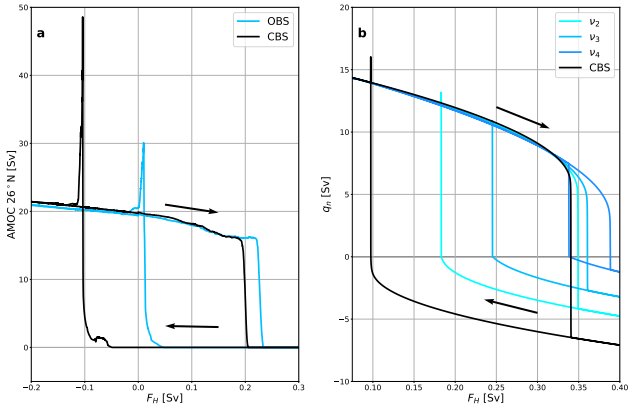

[t]

Figure 4. Hysteresis experiments where the freshwater forcing F_H is slowly increased with rate $dF_H/dt = \pm 0,025$ Sv/kyr beyond the occurrence of an AMOC collapse, and then reduced at the same rate till it recovers, for either OBS (blue) or CBS (black) in CLIMBER-X (**a**) shown by the AMOC strength at 26° N and in EWM (**b**) shown by q_n. For the latter setting $\nu = \in \{\nu_2, \nu_3, \nu_4\}$ (increasing shade of blue) and $q_0 = 14.25$ Sv are used. The arrows indicate direction of time. (**a**) is adapted from Soons and Dijkstra (2025).

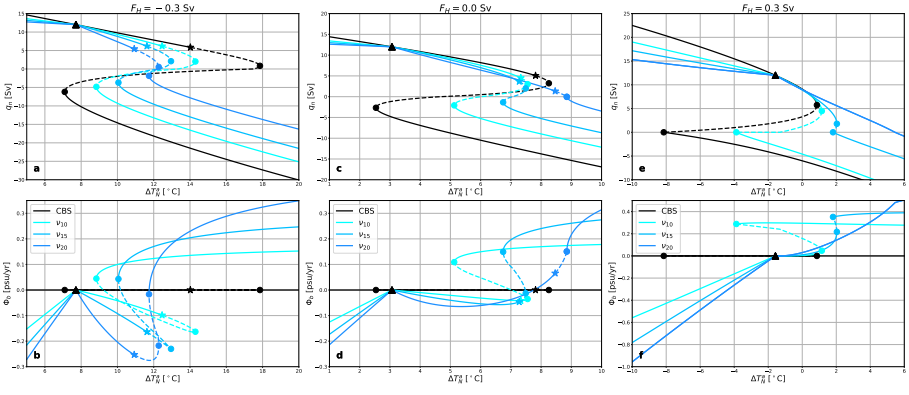

[t]

Figure 5. The bifurcation diagram of the EWM for increased Arctic amplification ΔT_N^a for the AMOC strength q_n (top row) and corresponding salinification effect of the BST on the *N* box Φ_b (bottom row) for either CBS (black), or OBS with parameters ν_{10}, ν_{15} or ν_{20} for increasing shade of blue with corresponding switching AMOC strength $q_0 = 12.0$ Sv, with fixed hosing strength F_H being -0.3 Sv, 0.0 Sv or 0.3 Sv (left to right column). Linearly stable branches (solid) and unstable branches (dashed) are connected by saddle-node bifurcations (dots) and Hopf bifurcations (asterisks). Triangles indicate where q_b switches sign.

strength $q_0 = 12.0$ Sv. As clarification, the salinification rate Φ_b of the northern box due to an open Strait is also shown, i.e.

$$\Phi_b = \begin{cases} q_b(S_A - S_N)/V_N & \text{if } q_b > 0, \\ |q_b|(S_B - S_N)/V_N & \text{if } q_b < 0. \end{cases} \tag{3}$$

https://doi.org/10.5194/egusphere-2025-6565
Preprint. Discussion started: 30 January 2026

The results in Figure 5 indicate that for low hosing strengths the tipping point due to Arctic amplification can be extended by a closure while the reverse is true for higher hosing strengths. The physical mechanism causing this is as follows: for low hosing values the northern box is still relatively saline as the AMOC approaches its temperature-induced tipping point and so the transport by the BST into the Indo-Pacific removes net salinity from the North Atlantic. As we can see in Figure 5b, after the BST has reversed the Strait still has a freshening effect on the North Atlantic ($\Phi_b < 0$ psu/yr), as relatively saline North Atlantic water is replaced by fresher bottom water (i.e. $S_N > S_B$). This destabilizes the AMOC. On the other hand, for a high hosing value and corresponding fresher North Atlantic the BST removes relatively fresh waters and replaces it by more saline bottom water (i.e. now $S_N < S_B$), and so it extends the temperature-induced tipping point. We see in Figure 5d that after the BST reversal the open Strait is freshening the *N* box, but for $\nu = \nu_{20}$ this turns into a salinifying effect ($\Phi_b > 0$ psu/yr) before the tipping point as S_N decreases. Hence here the open Strait extends the AMOC's tipping point under Arctic amplification. For larger values of ν and F_H this removal of freshwater Φ_b by the BST is even larger and can supplement the salinity loss due the reduction in advection enough to prevent the salt-advection feedback from developing, and hence the multi-stable regime disappears. Of course this reasoning only holds when the BST switches before the tipping point is reached, and so q_0 needs to be sufficiently high. Hence, we omit cases where $q_0 \leq 5.8$ Sv (see Figure 3), since for these cases F_H^1 increases under closure, which is indeed not found in CLIMBER-X and models of higher complexity (Hu et al., 2012, 2023).

The dependence of the bifurcation point $\Delta T_N^{a,1}$ for Arctic amplification with various AMOC switching strengths $q_0 \in \{6.5, 9.0, 12.0\}$ Sv is given in Figure 6. A closure extends the temperature-induced tipping point of the AMOC for low hosing values and reduces it for high hosing values. Note that case $q_0 = 12$ Sv with ν_{20} is omitted as for these there is no longer a multiple equilibria regime for varying northern atmospheric temperatures for all hosing strengths $F_H \in [-0.35, 0.35]$ Sv. We find that the difference with a closure is magnified for larger switching strengths q_0 and hydraulic parameter ν. This follows trivially, as for larger values of q_0 and ν the freshening (salinifying) effect of an OBS is also larger for the same high (low) AMOC strength corresponding to a low (high) hosing strength F_H. Furthermore, we can identify a critical hosing strength F_H^c below (above) which a closure extends (reduces) the temperature-induced tipping point. At the critical hosing strength F_H^c the temperature-induced tipping point under CBS and OBS overlap, since at this tipping point it holds that $\Phi_b = 0$ psu/yr. There the northern box's salinity and the bottom box's salinity are equalized and so the reversed BST ($q_b < 0$ Sv) has no net salinity transport to the northern box. Furthermore, the critical hosing strength is sensitively dependent on the chosen BST parameter (see Figure 6c) and it decreases with increasing q_0 and/or ν, since the BST's effect changes earlier to a larger salinifying effect (compare e.g. Figures 5 c-f). This is in particular the case for larger values of q_0 (while keeping percentage i in ν_i fixed), since for these the BST strength for a weakened AMOC is especially large. Hence, whether the temperature-induced tipping point is extended under CBS compared to the original OBS setting relies heavily on the chosen BST parameters, with both an AMOC BST switching strength or a larger response of the BST to an AMOC weakening resulting in a smaller freshwater range for which a closure is still effective.

https://doi.org/10.5194/egusphere-2025-6565
Preprint. Discussion started: 30 January 2026

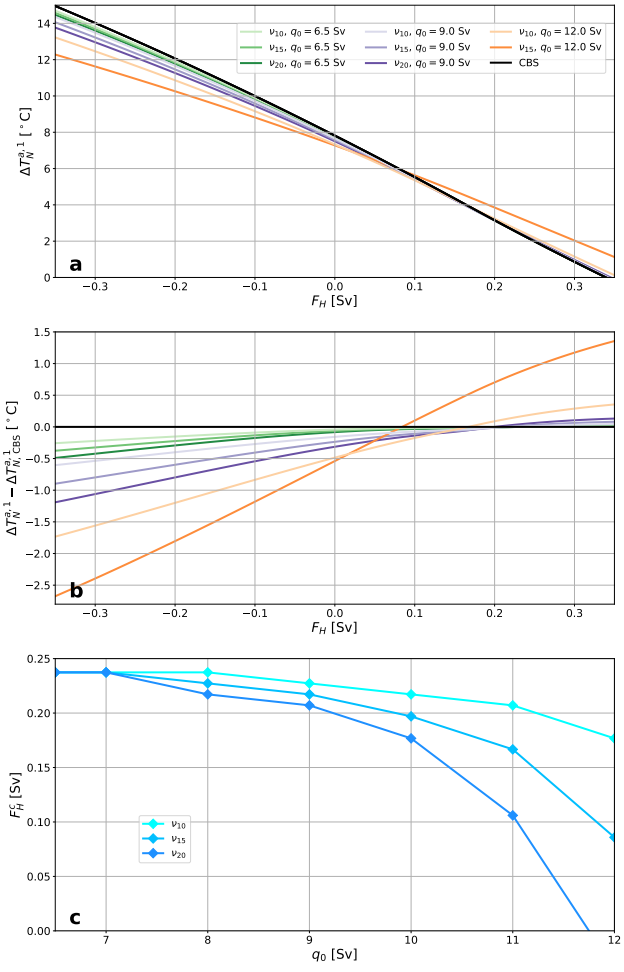

Figure 6. The temperature-induced bifurcation point $\Delta T_N^{a,1}$ of the EWM (**a**) under CBS (solid, black) and various combinations (ν, q_0) (solid, colored) for fixed hosing strength $F_H \in [-0.35, 0.35]$ Sv, with their respective difference with the CBS setting (**b**).

4 Closure experiments

A more real-world approach is now to force an equilibrium AMOC under OBS conditions and a fixed hosing strength with a time-dependent polar amplification. We subsequently implement a BSD as a climate intervention strategy. We examine for which conditions an immediate closure prevents an AMOC collapse and, if so, what the latest preventive closure time then is. Throughout this section the BST parameters are restricted to those following the tuning to CLIMBER-X: $q_0 = 14.25$ and $\nu \in \{\nu_2, \nu_3, \nu_4\}$, where ν is varied to test the sensitivity of the results. The choice to vary ν instead of q_0 is made, since then we get the largest variation in results (see also Figure 6c)

https://doi.org/10.5194/egusphere-2025-6565
Preprint. Discussion started: 30 January 2026

4.1 Immediate closure

First, we reproduce the closure experiment performed in CLIMBER-X as in Soons and Dijkstra (2025) with the EWM. The AMOC is forced by a time-dependent polar amplification following

$$T_N^a(t) = \begin{cases} T_N^{a,0} + \dfrac{\Delta T_N^{a,p}}{\cosh(r(t-T))}, & \text{for } t \in [0,T], \\ T_N^{a,0} + \Delta T_N^{a,p}, & \text{for } t > T. \end{cases} \tag{4}$$

which is based on the protocol described in Ritchie et al. (2023). Here the northern atmospheric temperature increases with rate r in time until it has increased to a peak $\Delta T_N^{a,p}$ at time T. This forcing is applied to the AMOC ON equilibrium for various fixed F_H under OBS, where we either keep the Strait open, or immediately close it at $t = 0$. The time $T = \left(20 + \log(\Delta T_N^a / 1°\text{C})\right)/r$, is fixed such that it always holds that $T_N^a(0) \approx T_N^{a,0}$. This yields for various freshwater forcings and BST parameter settings a critical peak $\Delta T_N^{a,c}$ for which the AMOC just collapses for either an open Strait or an immediate closure.

This is applied to the EWM with the previously mentioned BST parameters. The freshwater forcing range is limited to $F_H \in [-0.3, 0.3]$ Sv to avoid the freshwater-induced tipping point F_H^1. The forcing rate varies with $r \in \{0.1, 1, 10\}$/yr, where for rates outside this range no qualitative difference is observed. Additionally, the safe carbon budget of the AMOC in CLIMBER-X is shown as comparison for either an open Strait, or one that is immediately closed (Figure 7d).

Note that –regardless of a closure– a higher forcing rate r results in a lower critical amplitude $\Delta T_N^{a,c}$. This is because under a higher rate of forcing there is less time to transport excess heat out off the northern box, and so a higher oceanic temperature T_N –and correspondingly weaker AMOC– can be reached. That said, for higher hosing values an increased forcing rate seemingly does not alter the critical amplitude $\Delta T_N^{a,c}$ for neither OBS nor CBS. That is simply because close to the critical freshwater value F_H^1 the critical amplitudes $\Delta T_N^{a,c}$ are small, and so are their respective differences as well.

Now, regarding the effect of closure we see that an increased rate r affects the AMOC's resilience more with a closed Strait than with an open one. One can see from the insets in Figure 7a-c that the results from the previous bifurcation analysis still hold for the lowest rate $r = 0.1$/yr, with a CBS extending the tipping point for low hosing values. For higher rates this extension under low hosing values vanishes or even reverses, especially for larger values of ν. When a higher rate of forcing is applied, the AMOC strength q_n and northern salinity S_N decrease more rapidly, and hence the salinity contrast $S_B - S_N$ will be larger. Therefore the salinifying effect of the BST (Φ_b) will be larger for the same AMOC strength (and so for the same q_b) under higher forcing rates. Evidently, this stabilizing mechanism is absent under an immediate closure, and so the AMOC is less resilient to rate-induced tipping in the CBS configuration.

Changing BST parameter ν leaves the $\Delta T_N^{a,c}$-curves under CBS trivially unchanged. For the OBS setting we see that the differences with the CBS cases are amplified for larger ν, since the BST's effect is simply more prominent. Note furthermore that the previously described impact of an increased forcing rate is also larger for increased ν as the supplementing effect of the BST is now enhanced.

These results replicate the main result of Soons and Dijkstra (2025): an immediate closure increases the critical climate forcing needed to tip the AMOC for low hosing values and reduces it for high hosing values. As a qualitative comparison the

https://doi.org/10.5194/egusphere-2025-6565
Preprint. Discussion started: 30 January 2026

results in CLIMBER-X are also shown, with the precautionary mention that in Figure 7d global mean surface temperature (GMST) is shown on the ordinate as opposed to the polar amplification used in the EWM. For the tuned setting ($(q_0, \nu) = (14.25\text{ Sv}, \nu_2)$) we see a qualitative similarity for the higher forcing rates ($r \in \{1, 10\}$ /yr), where the CBS switches from stabilizing to destabilizing for a hosing strength relatively far from the tipping strength F_H^1. This is also the case for the low forcing rate once ν increases. An important difference is that the extension gained under CBS diminishes again for lower hosing strengths in CLIMBER-X, whereas it keeps increasing in the EWM. We suspect that for these low hosing values such a large amount of emissions is needed to collapse the AMOC in CLIMBER-X, that other destabilizing processes start to dominate and obscure the closure's effect. In the EWM this is not the case as all other parameters are fixed in time apart from the Arctic amplification. Furthermore, in Soons and Dijkstra (2025) a critical hosing value F_H^c (and corresponding critical equilibrium AMOC strength) was identified in this closure experiment. Based on the EWM results we can derive that such a value is not only highly dependent on the BST parameters but also on the rate of the applied forcing.

4.2 Delayed closure

Next, we use the EWM with $\nu(t)$ now a time-dependent variable to simulate a delayed closure of the Bering Strait at a time t_c

$$\nu(t) = \begin{cases} \nu_{\text{OBS}}, & \text{for } t < t_c, \\ 0, & \text{for } t > t_c, \end{cases}$$

and denote with t_c^f the last possible closure time that still prevents an AMOC tipping. When forcing profile (4) is adopted, we use $\Delta t_c^f = t_c^f - T$ for the time difference between the latest preventive closure and the forcing reaching its peak.

As a representative case, we start in the AMOC ON equilibrium with fixed $F_H = -0.2$ Sv, and $q_0 = 14.25\ Sv$ and $\nu = \nu_2$ (i.e. tuned to CLIMBER-X). The AMOC is forced with an Arctic amplification following (4) with $r = 1$/yr and $\Delta T_N^{a,p} = 8.6°$C, which corresponds to $\Delta t_c^f = -0.06$ yr, i.e. the last preventive closure is just before the forcing peaks at $T = 22.15$ yr. We vary the closure time with $t_c \in [0, 30]$ yr, and so part of the trajectories will see a recovered AMOC while the other part sees a collapsed one (Figure 8). Additionally, an OBS trajectory (i.e. without a closure) is generated as a reference

Clearly, the latest possible preventive closure needs to occur before the freshening effect of the OBS switches to a salinifying effect on the northern box (i.e. $\Phi_b \lessgtr 0$ psu/yr, see Figure 8c). As the AMOC weakens, so does q_b and so does the freshening effect $-\Phi_b$, till eventually the BST switches sign. From thereon the BST still has a net freshening effect, since it exports relatively saline waters from the northern box. Only at $t = 25.1$ yr has S_N sufficiently decreased that the export induced by the BST has a net salinifying result. Closures occurring after this switch have directly a freshening effect on the northern box, and their corresponding AMOC strength decreases quicker compared to the OBS reference trajectory (see Figures 8a-b). Note that closures occurring after t_c^f but before the switch in Φ_b cause initially the same salinifying pattern as the recovering trajectories, and a corresponding slow-down in AMOC decrease. However, eventually the developing salt-advection feedback overcomes this stabilizing impulse, and the AMOC strength then sees a steeper decline w.r.t. the OBS reference, since before the latter reaches its OFF-state the BST has again a salinifying effect ($\Phi_b > 0$ psu/yr). As additional clarification Figure E1 replicates Figures 8a-b, where now the trajectories are partitioned based on whether a closure occurs before t_c^f, between t_c^f and

https://doi.org/10.5194/egusphere-2025-6565
Preprint. Discussion started: 30 January 2026

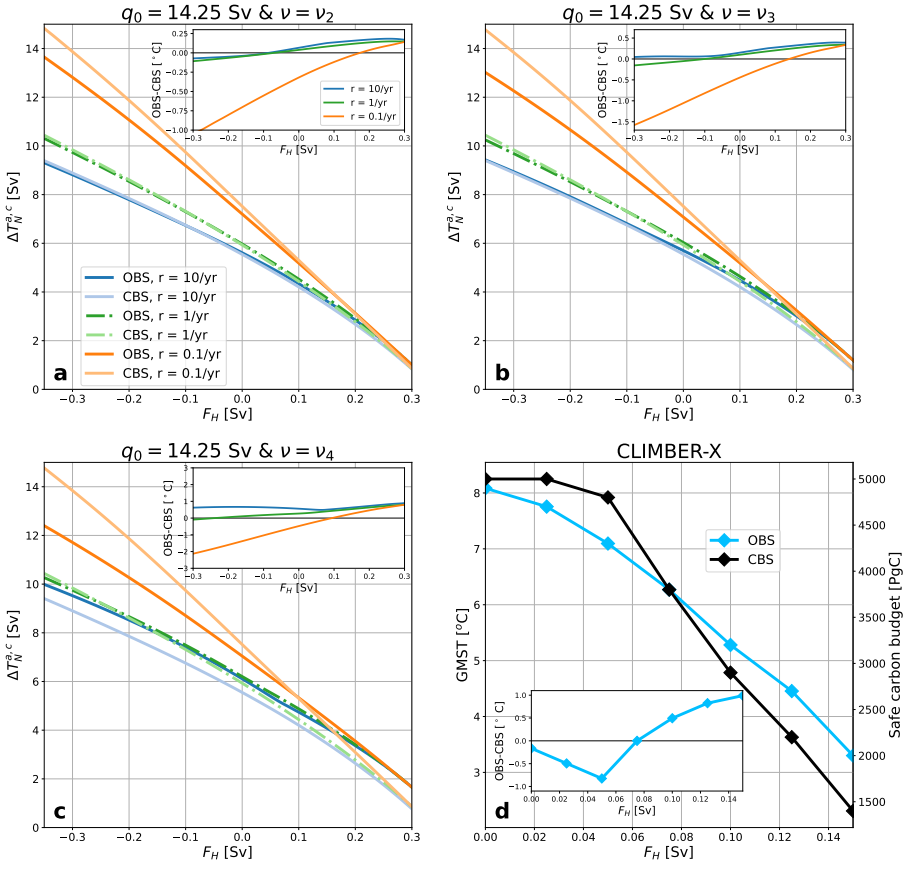

Figure 7. The critical peak temperature $\Delta T_N^{a,c}$ for which an AMOC ON state just collapses with BST settings $q_0 = 14.25$ Sv and $\nu = \nu_2$ (**a**), $\nu = \nu_3$ (**b**), and $\nu = \nu_4$ (**c**) with rates $r \in \{0.1, 1, 10\}$/yr (orange, green, blue) where either the Strait is kept open (OBS, non-transparent) or immediately closed (CBS, semi-transparent) for various fixed hosing strengths F_H. The safe carbon budget of the AMOC in CLIMBER-X (**d**) for various fixed hosing strengths F_H, where either the strait is immediately closed (CBS, black) or kept open (OBS, blue), is on the right vertical axis. The corresponding increase in global mean surface temperature (GMST) is on the left vertical axis, using 1.65°C/1000 PgC (Canadell et al., 2021). The insets show the respective difference between the results for the CBS and OBS setting, with either the difference in $\Delta T_N^{a,c}$ (insets **a**-**c**) or the difference in GMST (inset **d**). (**d**) is adapted from Soons and Dijkstra (2025).

the moment where the open Strait starts salinifying the North Atlantic ($\Phi_b \lesseqgtr 0$ psu/yr), and after the open Strait is salinifying $\Phi_b > 0$.

330 A projection of the trajectories onto $(S_T, S_N)-$space is done, since the trajectories exhibit the largest variations in these two dimensions (Figure 8f). Moreover, for the original model, Alkhayuon et al. (2019) found that in this space recovering (collapsing) trajectories show a characteristic anti-clockwise (clockwise) curvature, similarly to our trajectories in the EWM. As the AMOC weakens S_N decreases naturally, whereas S_T increases because less of its salinity is transported northward. A combination of low S_N and high S_T can still result in a recovery, as salinity from the T box supplements the northern density

https://doi.org/10.5194/egusphere-2025-6565
Preprint. Discussion started: 30 January 2026

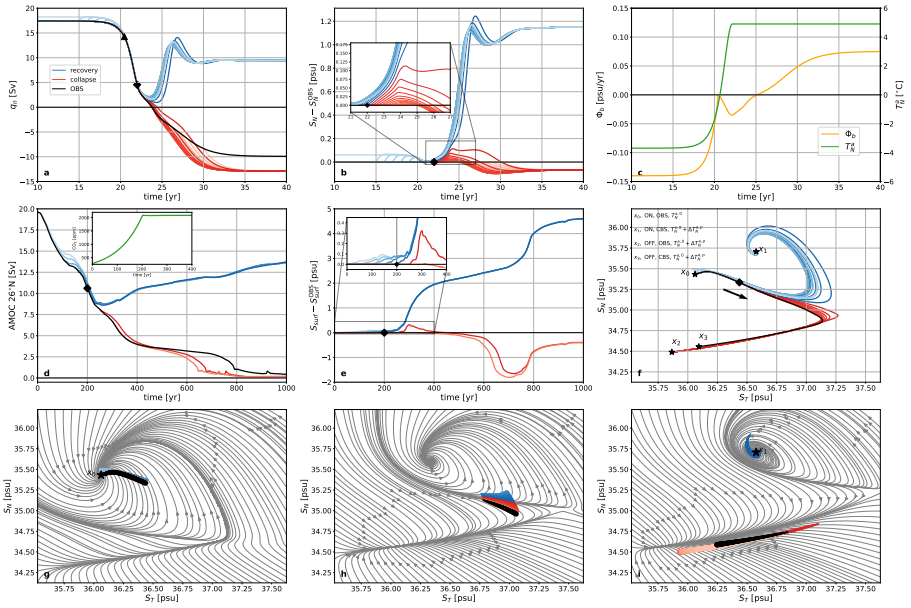

Figure 8. Multiple trajectories for $F_H = -0.2$ Sv, and $q_0 = 14.25\ Sv$ and $\nu = \nu_2$ in the EWM that are forced following (4) with $r = 1$/yr and $\Delta T_N^{a,p} = 8.6°$C for various closure times $t_c \in [0, 30]$ yr, with recovering trajectories (blue, darker shade for later closure), collapsing trajectories (red, darker shade for earlier closure), and a trajectory without closure (OBS, black): the AMOC strength vs. time (**a**), the northern salinity S_N difference w.r.t. the OBS setting vs. time (**b**), and northern salinity S_N vs. S_T (**f**) of the trajectories are shown. Additionally, the salinifying effect Φ_b (see equation (3)) of the OBS trajectory is shown (orange, **c**), and the temperature forcing T_N^a (green, **c**). The triangle, diamond, and arrow indicate the reversal of the BST, the latest preventive closure, and direction of time, respectively. Streamlines of the vector field expanded around the recovering trajectory with the latest preventive closure evaluated at $t = 10$ yr (**g**), at $t = 24$ yr (**h**), and $t = 40$ yr (**i**) in (S_T, S_N)-space, with the trajectories superimposed for time intervals $t \in [0, 22]$ yr (**g**), $t \in [23, 24]$ yr (**h**), and $t \in [27.5, 32]$ yr (**i**). Several (linearly) stable equilibria are denoted by x_i. In CLIMBER-X the AMOC is forced with 4900 PgC of emissions and no additional hosing, and subsequently the Strait is closed for various closure times $t_c \in [0, 300]$ yr accompanied by an OBS reference case (same color scheme as in (**a**)), shown as the AMOC strength at 26°N vs. time (**d**) and as the difference in North-Atlantic surface salinity $S_{\mathbf{surf}}$ w.r.t. the OBS reference vs. time (**e**). The inset in (**d**) is the corresponding CO_2-forcing. (**d**) and (**e**) are adapted from Soons and Dijkstra (2025).

loss via the subtropical gyre (Soons et al., 2024). Four (linearly) stable equilibria are denoted. State x_0 is the original starting state with an AMOC ON state under OBS without additional polar amplification; x_1 is an AMOC ON state under CBS with the northern atmospheric temperature increased by $\Delta T_N^{a,p}$; and x_2 and x_3 are the AMOC OFF states for this increased temperature under OBS and CBS, respectively.

For times $t_i \in \{10, 24, 40\}$ yr we plot the instantaneous vector fields in S_T and S_N, where we assume the other state variables to be fixed at the values attained at t_i by the recovery trajectory with the latest closure, see Figures 8g-i. These provide an approximate overview of the stability landscape around the recovering trajectories. The initial state x_0 is a stable node from which the trajectories are forced out off by the Arctic amplification. In Figure 8g the maximum increase in atmospheric

https://doi.org/10.5194/egusphere-2025-6565
Preprint. Discussion started: 30 January 2026

temperature has been reached, and the trajectories lie around the basin boundary of the ON and OFF state. The recovering trajectories have had a sufficiently large increase in S_N by the closure to be in the basin of attraction of the ON state. Note that in time the two sets of trajectories increasingly deviate from the basin boundary, as the salt-advection feedback will drive either the recovering trajectories to the ON-state (x_1) or the collapsing trajectories away to the OFF-state (see Figure 8i). Note that the collapsing trajectories slightly deviate from the instantaneous vector field, as the latter is based on the attained variables by a recovering trajectory.

Hence considering t_c^f there are two restraining effects. Firstly, the salinification effect of a closure compared to the reference OBS diminishes over time as the AMOC weakens. And secondly, in time the needed salinity input to force a trajectory into the basin of attraction of the ON-state grows. This causes the switching time of Φ_b to be only an upper bound.

We compare the trajectories in the EWM in figures 8a-b to those in CLIMBER-X in figures 8d-e, where the latter ones were forced with 4900 PgC of emissions and no freshwater hosing. Subsequently, the Strait was closed at times $t_c \in \{0, 50, 100, 150, 200, 250, 300\}$ yr, and it was found that the latest preventive closure time is at 250 yr after the forcing starts. Two qualitative similarities can be seen between the trajectories in the EWM and CLIMBER-X. Firstly, a closure that is marginally too late also sees the initial salinifying effect of the North Atlantic by a closure, which is eventually halted by the salt-advection feedback. The corresponding AMOC weakening is then initially slower w.r.t. the OBS reference trajectory, before it overtakes it again. Secondly, a closure that is substantially later than t_c^f sees an immediate freshening of the North Atlantic and corresponding more rapid decrease in AMOC strength. The most prominent qualitative difference between the two sets of trajectories is in the manner of recovery. In CLIMBER-X the recovery in AMOC strength is gradual, whereas in the EWM it is as fast as the initial decline. This could again be related to other destabilizing processes occurring in the EMIC, causing the AMOC to have a longer recovery. Apart from that, there are some quantitative differences, where mainly the time scale and the salinity differences are an order of magnitude smaller in the EWM. A slower rate of forcing in the EWM would yield a more comparable time scale to the EMIC, but also results in oscillatory behaviour of the AMOC which is no longer qualitatively comparable to CLIMBER-X. This will be discussed at the end of this section.

Again we check the sensitivity of our results with respect to the choice of BST parametrization. We force the initial AMOC ON state with varying hosing strengths $F_H \in [-0.3, 0.0]$ Sv and let $\Delta T_N^{a,p}$ be the average of the critical amplitude under OBS and under an immediate closure. We adopt the same BST settings as in Figure 7 and fix $r \in \{0.1, 0.5, 1.0, 2.5\}$ Sv such that a closure can prevent a collapse for a fraction of the considered freshwater strengths. The time difference Δt_c^f between the last preventive closure and the onset of the maximum atmospheric temperature T_N^a is plotted in Figure 9a, and the ratio of the corresponding AMOC strength at the latest preventive closure q_n^c to the starting equilibrium AMOC strength q_n^0 under OBS circumstances is plotted in Figure 9b. Note that only forcing cases for which a closure prevents a collapse are shown. The timing of the latest preventive closure mainly relies on the rate of forcing: for a lower rate of forcing the closure has to occur farther ahead of when the maximum temperature is reached. When the temperature increases more slowly, the AMOC is already weakened and S_N has already decreased before T_N^a reaches its maximum, and so a relatively earlier closure is needed. On the other hand, for a high rate of forcing the latest closure can occur close to the moment of peak forcing, but the AMOC strength still has to be close to its original starting level. As for such high rates the density ρ_N drops quickly, giving little time

https://doi.org/10.5194/egusphere-2025-6565
Preprint. Discussion started: 30 January 2026

for other adjustments that help stabilize the AMOC such as an increased salinity of the Atlantic thermocline and a higher heat content in the Southern Ocean (Soons et al., 2025). Hence, only a relatively strong AMOC can then still be saved.

Moreover, for an increased ν an earlier closure is needed with an corresponding stronger AMOC, since the destabilizing effect of the OBS is then larger. This effect diminishes with increased rate, as previously seen in Figure 7. Thirdly, the freshwater forcing F_H has relatively little influence on Δt_c^f and the corresponding AMOC strength, since far away from the freshwater-induced tipping point it has only limited effect on the AMOC's stability.

Note that in Figures 9a-b only a limited range of forcing rates is considered. For rates higher than considered ($r > 2.5$/yr) the latest preventive closure needs to occur before substantial weakening occurs ($q_n^c/q_n^0 \to 1$), since the added salinification of a closure is limited due to the rapid AMOC weakening (Figure 9c). Increasing rates only result in Δt_c^f converging to a limit, and are hence omitted from the figure. Lower rates ($r < 0.1$/yr) are also not shown. At these rates the forced trajectory is in quasi-equilibrium and hits the Hopf-bifurcation (see Figures 5a-d), resulting in the OBS trajectory oscillating before the AMOC collapse (Figures 9d-f). During such an oscillation a weakened AMOC results in a build-up of salinity in the T box, which in turn supplements S_N via the gyre resulting in an increased AMOC strength. This in turn removes salinity from the Atlantic thermocline again. How many oscillations occur depends on the forcing rate and freshwater strength F_H, and hence greatly affects time t_c^f.

5 Discussion

In this study we introduced an extension of the conceptual model proposed by Wood et al. (2019). It includes ocean and atmospheric temperatures in order to enable a temperature-induced tipping of the AMOC via an Arctic amplification. Moreover, the effect of an open Bering Strait has been included by adding a connection between the boxes that represent the Indo-Pacific and North Atlantic. The strength and direction of the BST is directly coupled to the AMOC strength according to existing theory (Cessi, 2020). This model allows us to asses conceptually the effect of a Bering Strait closure on the AMOC's resilience to tipping under climate change. Additionally, we compared the model's results qualitatively to those found in an earlier study using the EMIC CLIMBER-X (Soons and Dijkstra, 2025).

A bifurcation analysis for varying freshwater forcing F_H showed that if the BST reverses for a sufficiently large AMOC strength the AMOC is more resilient to large freshwater perturbations in the Atlantic than under a closure of the Strait. In this case the additional freshwater perturbations are partially removed by the BST to the Indo-Pacific. Moreover, for certain BST parameter values this removal is sufficiently strong to prevent the salt-advection feedback from developing causing the AMOC's multi-equilibrium regime to vanish.

The bifurcation analysis for varying increases ΔT_N^a of the northern atmospheric temperature is performed for a range of BST parameters for which a closure reduces the critical hosing strength F_H^1, in agreement with previous literature (De Boer and Nof, 2004; Hu et al., 2012, 2023). It highlights the AMOC's resilience to an Arctic amplification induced by climate change, and reveals that a closure can stabilize the AMOC and prevent a temperature-induced collapse provided a low enough freshwater forcing. The underlying mechanism is that for low freshwater forcing –and correspondingly a relatively saline northern box– a

https://doi.org/10.5194/egusphere-2025-6565
Preprint. Discussion started: 30 January 2026

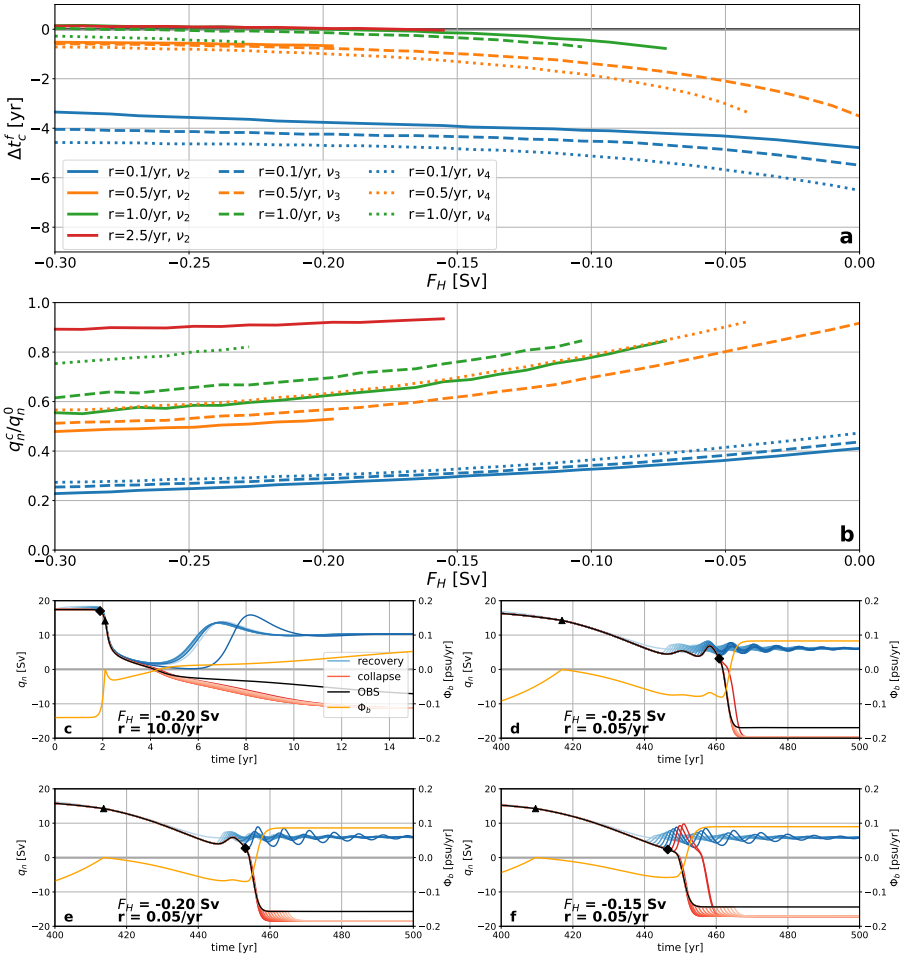

Figure 9. The time difference Δt_c^f between the latest preventive closure and the attainment of the maximum temperature T_N^a for various hosing strengths $F_H \in [-0.3, 0.0]$ Sv for rates $r \in \{0.1, 0.5, 1.0\}$ /yr (blue, orange, green) with $q_0 = 14.25$ Sv and $\nu \in \{\nu_2, \nu_3, \nu_4\}$ (solid, dashed, dotted) (**a**). The AMOC strength q_n of multiple trajectories in the EWM with $q_0 = 14.25\ Sv$ and $\nu = \nu_2$ for various closure times that are forced following (4) with $r = 10$/yr, $\Delta T_N^{a,p} = 7.85°$C and $F_H = -0.20$ Sv (**b**), $r = 0.05$/yr, $\Delta T_N^{a,p} = 12.72°$C and $F_H = -0.25$ Sv (**c**), $r = 0.05$/yr, $\Delta T_N^{a,p} = 11.76°$C and $F_H = -0.15$ Sv (**d**), $r = 0.05$/yr, $\Delta T_N^{a,p} = 10.76°$C and $F_H = -0.15$ Sv (**e**), with recovering trajectories (blue, darker shade for later closure), collapsing trajectories (red, darker shade for earlier closure), and a trajectory without closure (OBS, black). Additionally, the salinifying effect Φ_b (see equation (3)) of the OBS trajectory is shown (orange, **b-d**). The triangle and diamond indicate the reversal of the BST and the latest preventive closure, respectively.

reversal of the BST due to temperature-induced weakening of the AMOC actually causes a net freshening of the North Atlantic, and hence destabilizes the AMOC. In this case a closure would aid its resilience. The critical hosing strength and corresponding AMOC strength under which this holds, are sensitively dependent on the parameter choice for the BST.

https://doi.org/10.5194/egusphere-2025-6565
Preprint. Discussion started: 30 January 2026

A BSD was implemented to trajectories originating from the ON-state under OBS conditions. For a closure at the start of the forced trajectory it follows that again the BSD's effectiveness greatly relies on the choice of BST parameters, with an increase in ν resulting in a diminished freshwater regime for which a closure stabilizes AMOC, similarly as the bifurcation analysis. Moreover, an increased rate of forcing reduces or even reverses the extension by the closure. The timing of the last preventive closure is also mainly influenced by the rate of the applied forcing, with a closure already needed when the AMOC is still as strong as initially for high rates, while for low rates a closure can still result in a recovery despite the AMOC being already severely weakened. Hence for a time-dependent forcing a critical AMOC strength above which the closure must occur, is specific for the rate of forcing.

The conceptual model results were compared to the results obtained in Soons and Dijkstra (2025) using the EMIC CLIMBER-X. The freshwater hysteresis experiment as well as both closure experiments can be qualitatively reproduced in the EWM, showing that a relatively simple formulation of the BST's feedback onto the AMOC can explain these results. Moreover, it indicated that these results –including a critical hosing value F_H^c– are dependent on the parameter value of the BST and temperature forcing rate. Hence, the EMIC's results might also rely sensitivity on the model parameters, and must therefore be verified in a more-detailed model as a next step. We do expect a Bering Strait closure to be more effective in these models under RCP-scenarios than in Soons and Dijkstra (2025), since in CLIMBER-X the effect of a closure is relatively small at only a 2% increase in AMOC strength under pre-industrial conditions, while the CO_2 concentration increased at the relatively large rate of 1%/yr.

The foremost limitation of this study is the simplicity of the adopted model. The coupling between the AMOC and BST is assumed to be direct with a weakening in the BST affecting the salinity in the Northern Atlantic immediately. Any delay in transport or storage in the Arctic has been omitted for the sake of simplicity. Also, this choice is consistent with previous conceptual models linking the BST to the AMOC (Shaffer and Bendtsen, 1994; De Boer and Nof, 2004). Moreover, we have assumed that any transport through the relatively fresh upper Arctic has a fixed salinity S_A. This way an additional set of evolution equations for an Arctic box could be omitted. Furthermore, the effect of the BST onto the North Atlantic can then be aggregated into one parametrization, which avoids additional assumptions regarding the impact of a closure on the Arctic-Atlantic freshwater exchange. This fixed Arctic salinity is likely unrealistic under a severely weakened or collapsed AMOC, where the increased sea-ice formation will salinify the upper Arctic Ocean via brine rejection. However, in this study we mainly discussed the tipping point of the AMOC ON state, where this limitation is less severe as for the OFF state. Also, varying S_A only affected the results quantitatively.

The extension with atmospheric heat forcing contains simplifying assumptions too. The omission of any effect of the oceanic temperatures back onto the atmosphere can result in unchanged atmospheric temperatures despite a collapsed AMOC. However, as just stated, this study mainly focused on the tipping point of the AMOC ON state. Secondly, we captured the destabilizing effect of climate change on the AMOC through polar amplification of atmospheric temperatures (Dai, 2022), which omits other significant effects such as shifting precipitation patterns or Greenland Ice Sheet melt (Sasgen et al., 2020; Van Westen and Dijkstra, 2023). Lastly, in testing the AMOC's resilience we have neglected to include stochastic forcing. Although the

https://doi.org/10.5194/egusphere-2025-6565
Preprint. Discussion started: 30 January 2026

original model has been extended to include noisy forcing (Chapman et al., 2024), this had little effect on its stability when the system is away from its freshwater-induced tipping point, and is therefore not considered in this study.

All in all, this work provides a conceptual framework for the closure of the Bering Strait in preventing an AMOC collapse with a climate box model that can qualitatively reproduce the results from Soons and Dijkstra (2025). The results will also be important for the interpretation of future simulations studying the effect of the BSD on the stability of the AMOC using Earth System Models. The latter results will be crucial to evaluate whether a BSD can be a potential effective climate intervention strategy in order to prevent an AMOC tipping, should greenhouse emissions reductions prove to be insufficient.

Code and data availability. The results can be readily reproduced using the described method and the stated parameter values. The code for the box model and bifurcation analysis can be obtained via https://doi.org/10.5281/zenodo.17977683.

Appendix A: Model equations

The salinity evolution equations are as follows

$$V_N\frac{dS_N}{dt} = q_n\Big(\theta(q_n)(S_T-S_N)-\theta(-q_n)(S_B-S_N)\Big)+K_N(S_T-S_N)-F_NS_0+C_NF_HS_0 + q_b\Big(\theta(q_b)(S_A-S_N)-\theta(-q_b)(S_B-S_N)\Big) \tag{A1a}$$

$$V_T\frac{dS_T}{dt} = q_n\Big(\theta(q_n)(\gamma S_S+(1-\gamma)S_{IP}-S_T)-\theta(-q_n)(S_N-S_T)\Big)+K_S(S_S-S_T) - F_TS_0+C_TF_HS_0 \tag{A1b}$$

$$V_S\frac{dS_S}{dt} = \gamma q_n\Big(\theta(q_n)(S_B-S_S)-\theta(-q_n)(S_T-S_S)\Big)+K_{IP}(S_{IP}-S_S)+K_S(S_T-S_S)+\eta(S_B-S_S) - F_SS_0+C_SF_HS_0 \tag{A1c}$$

$$V_{IP}\frac{dS_{IP}}{dt} = (1-\gamma)q_n\Big(\theta(q_n)(S_B-S_{IP})-\theta(-q_n)(S_T-S_{IP})\Big)+K_{IP}(S_S-S_{IP})-F_{IP}S_0+C_{IP}F_HS_0 + q_b\Big(\theta(q_b)(S_B-S_{IP})-\theta(-q_b)(S_A-S_{IP})\Big) \tag{A1d}$$

$$V_B\frac{dS_B}{dt} = q_n\Big(\theta(q_n)(S_N-S_B)-\theta(-q_n)(\gamma S_S+(1-\gamma)S_{IP}-S_B)\Big)+\eta(S_S-S_B)+|q_b|\Big(S_N+S_{IP}-S_A-S_B\Big) \tag{A1e}$$

where S_0 is a reference salinity and $\theta(x)$ the Heaviside function. Since salinity is conserved any of these salinities can also be diagnostically determined via

$$\langle S\rangle = \frac{V_NS_N+V_TS_T+V_SS_S+V_{IP}S_{IP}+V_BS_B}{V_N+V_T+V_S+V_{IP}+V_B}. \tag{A2}$$

https://doi.org/10.5194/egusphere-2025-6565
Preprint. Discussion started: 30 January 2026

The heat content evolution equations are as follows

$$V_N \frac{dT_N}{dt} = q_n\Big(\theta(q_n)(T_T - T_N) - \theta(-q_n)(T_B - T_N)\Big) + K_N(T_T - T_N) - \mu^a A_N(T_N - T_N^a) \tag{A3a}$$

$$V_T \frac{dT_T}{t} = q_n\Big(\theta(q_n)(\gamma T_S + (1-\gamma)T_{IP} - T_T) - \theta(-q_n)(T_N - T_T)\Big) + K_S(T_S - T_T) - \mu^a A_T(T_T - T_T^a) \tag{A3b}$$

$$V_S \frac{dT_S}{dt} = \gamma q_n\Big(\theta(q_n)(T_B - T_S) - \theta(-q_n)(T_T - T_S)\Big) + K_{IP}(T_{IP} - T_S) + K_S(T_T - T_S) + \eta(T_B - T_S) - \mu^a A_S(T_S - T_S^a) \tag{A3c}$$

$$V_{IP} \frac{dT_{IP}}{dt} = (1-\gamma)q_n\Big(\theta(q_n)(T_B - T_{IP}) - \theta(-q_n)(T_T - T_{IP})\Big) + K_{IP}(T_S - T_{IP}) - \mu^a A_{IP}(T_{IP} - T_{IP}^a) \tag{A3d}$$

$$V_B \frac{dT_B}{dt} = q_n\Big(\theta(q_n)(T_N - T_B) - \theta(-q_n)(\gamma T_S + (1-\gamma)T_{IP} - T_B)\Big) + \eta(T_S - T_B) \tag{A3e}$$

where now none can be replaced by a diagnostic equation since the total heat content is not conserved.

Appendix B: Determining parameters for atmospheric heating

The surface area A_i of box i is determined by dividing the box's volume V_i by a characteristic height H_i. As boxes *T*, *S* and *IP* describe surface water masses we use $H_i \approx 1000$m for $i \in \{T, S, IP\}$ as this is a typical thermocline depth, while box *N* describes NADW which sinks to depths of $H_N \approx 4000$m (Talley, 2011).

For the heat exchange parameter a range of values is employed with $\mu^a \in [3 \cdot 10^{-6}, 15 \cdot 10^{-6}]$ m/s, which corresponds to $\rho_0 c_p \mu^a \in [12.0, 59.9]$ W/(m$^2 \cdot K$). This is a relatively large range as estimates for sensible heat fluxes can vary greatly with e.g. wind speeds and air density (Bonino et al., 2022). Typical values range from 20 W/(m^2·K) to 65 W/(m^2·K), with 30 W/(m^2·K) often used (Sein et al., 2015). For each μ^a the atmospheric temperatures are found by demanding that the salinity values and temperatures T_N and T_S for an equilibrium AMOC state without hosing ($q_n > 0$ Sv and $F_H = 0$ Sv) are equal to those in the equilibrium state of the original model. Note that fixing T_N and T_S to their old values already fixes q_n and the salinities via equations (A1a) to (A1e). Furthermore T_B is then also determined via equation (A3e), leaving the four remaining equations (A3a) to (A3d) to derive the atmospheric temperatures and T_N and T_{IP}. Hence two additional constraints are needed. We demand that T_{IP}^a equals T_T^a, and we fix the average atmospheric temperature $\langle T_a \rangle$.

The results for various μ^a and $\langle T^a \rangle$ are depicted in Figure B1. One can see that for increasing μ^a the atmospheric and oceanic temperature of each box asymptotically approach each other, since for increasing μ^a any anomaly in the oceanic temperature will be progressively more damped and forced towards the fixed atmospheric temperature. This also means that in the limit $\mu^a \to \infty$ all oceanic temperatures will be fixed as well. Note also that the *N* and *S* boxes are cooled by the atmosphere, while the *T* and *IP* boxes see a slightly warmer atmosphere above them. In order to maintain the original temperatures T_N and T_S despite the transport of warm waters from the Atlantic and Indo-Pacific thermocline boxes the high-latitudinal boxes need to be cooled. In particular the *N* box sees a much cooler atmosphere, as the active AMOC transports warm waters into it, while at the same time its available surface area A_N for cooling is relatively small. In particular for low values of μ^a the atmospheric temperature T_N^a must be unrealistically low. For the *T* and *IP* boxes is the exact opposite: the warmer atmosphere above them is

https://doi.org/10.5194/egusphere-2025-6565
Preprint. Discussion started: 30 January 2026

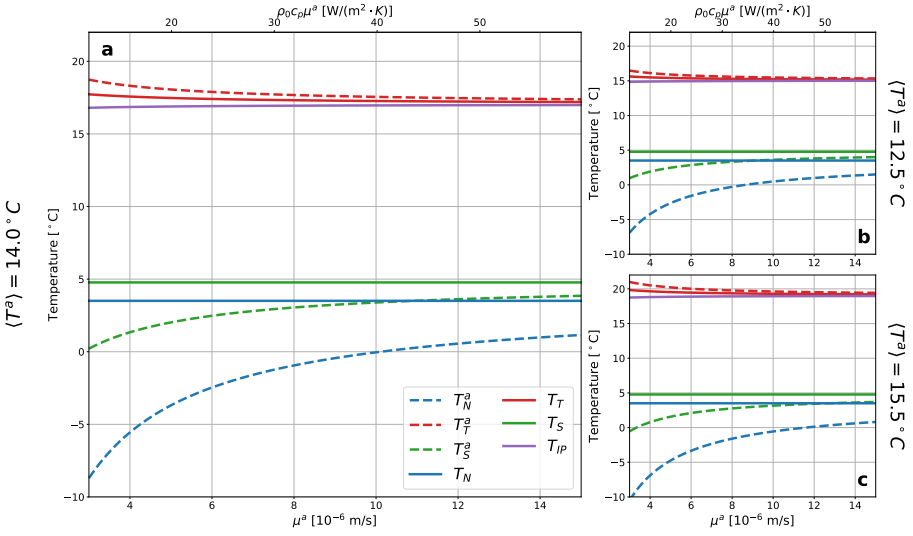

Figure B1. The atmospheric temperatures T_N^a (blue, dashed), T_T^a (red, dashed) and T_S^a (green, dashed), and the oceanic temperatures T_N (blue, solid), T_T (red, solid), T_S (green, solid) and T_{IP} (purple, solid) for a range $\mu^a \in [3.5 \cdot 10^{-6}, 15 \cdot 10^{-6}]$m/s with (**a**) $\langle T^a \rangle = 13.5°$C, or (**b**) $\langle T^a \rangle = 12.5°$C, or (**c**) $\langle T^a \rangle = 15.5°$C.

needed to compensate for the imported cold waters from the *N* and *S* boxes, but the atmosphere-ocean temperature gradient is only marginal as the surfaces A_T and in particular A_{IP} are relatively large. When considering the sensitivity of the results to a change in the average atmospheric temperature $\langle T^a \rangle$ we see that a larger $\langle T^a \rangle$ leads to slightly lower temperatures T_N^a and T_S^a, but mainly results in an increase in temperatures T_T^a, T_{IP} and T_T. This follows from the fact that the northern and southern box still need to be cooled in order to obtain their original temperatures T_N and T_S, and so a higher average temperature mainly leads to an increase in the other temperature variables.

Furthermore, we test the effect of these parameter changes on the dynamical behaviour of the system by computing the bifurcation diagrams of q_n and T_N for a varying hosing strength F_H, see Figure B2. The employed atmospheric parameters are listed in table B1. We can see that the changes in behaviour are only quantitative. A larger μ^a or lower $\langle T^a \rangle$ results in a reduced critical hosing value for an AMOC collapse. For these T_N^a are not as low and so the reduction in T_N is not as large under AMOC weakening. Hence a weakening AMOC sees a smaller increase in density of the northern box via this thermal feedback mechanism in order to stabilize itself. Note that for a too low μ^a or too high $\langle T^a \rangle$ the northern oceanic temperature under a collapsed AMOC is unrealistically low. On the other hand, a low estimate for μ^a this leads to a larger thermal response under an AMOC collapse. Therefore we take as parameter values $\mu^a = 5.0 \cdot 10^{-6}$m/s ($\rho_0 c_p \mu^a \approx 20$W/(m^2·K)) and $\langle T^a \rangle = 14°$C as found in literature (Inglis et al., 2020; Sein et al., 2015). A more detailed analysis of the effect of the heat-exchange parameter on the bifurcation structure of the AMOC can be found in Van Westen et al. (2024a).

https://doi.org/10.5194/egusphere-2025-6565
Preprint. Discussion started: 30 January 2026

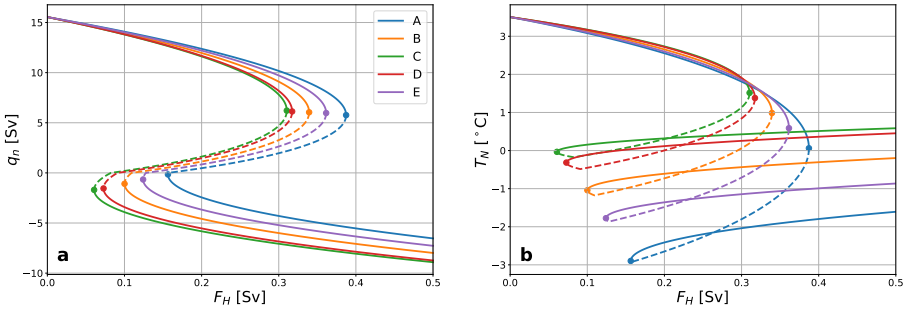

Figure B2. The bifurcation diagrams for cases A (blue), B (yellow), C (green), D (red) and E (purple) with stable branches (solid) and an unstable branch (dashed) for varying hosing strength F_H with on the ordinate AMOC strength q_n (**a**) or temperature of the northern box T_N (**b**). The dots indicate a saddle-node bifurcation. The parameters of the cases can be found in table B1.

Table B1. Atmospheric parameter values, where case B is used for the main results of this study.

	$\langle T^a \rangle$ [°C]	μ^a [$\cdot 10^{-6}$ m/s]	T^a_N [°C]	T^a_T [°C]	T^a_S [°C]	T^a_{IP} [°C]
A	14.0	3.5	-6.8991	18.4965	0.8556	18.4965
B	14.0	5.0	-3.6924	18.0611	2.0201	18.0611
C	14.0	6.5	-1.9942	17.8264	2.6507	17.8263
D	12.5	5.0	-2.6306	15.9080	2.4727	15.9080
E	15.5	5.0	-4.7541	20.2142	1.5675	20.2142

Appendix C: Extended Wood Model parameters

The parameters used in the EWM consist of those used in the original model following the calibration to the *FAMOUS*$_B$ 1×CO_2 experiment (Wood et al., 2019), and the previously determined atmospheric parameters, see Table C1.

Appendix D: BST parameter values

In figure D1 the equilibrium AMOC strengths under no-hosing ($F_H = 0$ Sv) for several values of (v, q_0) are depicted, together with the curves $\nu_{20}(q_0)$, $\nu_{15}(q_0)$ and $\nu_{10}(q_0)$. Several values on these curves are given in table D1, together with the values resulting from the tuning to CLIMBER-X. Note that we impose $q_0 \leq 12.5$ Sv when considering the curves $\nu_{20}(q_0)$, $\nu_{15}(q_0)$ and $\nu_{10}(q_0)$: the equilibrium AMOC strength without hosing is 15.5 Sv under CBS, and hence this limit is needed otherwise there would already be a flipped BST under no hosing for ν_{20} for an open Strait.

Appendix E: Additional figures

Additional figures consist of Figure E1.

https://doi.org/10.5194/egusphere-2025-6565
Preprint. Discussion started: 30 January 2026

Table C1. Parameter values of the EWM

parameter	value	description	parameter	value	description
V_N [10^{16} m^3]	3.261	volume *N* box	F_{IP} [Sv]	-0.739	freshwater flux into *IP* box
V_T [10^{16} m^3]	7.777	volume *T* box	$\langle S \rangle$ [psu]	35	average salinity in basin
V_S [10^{16} m^3]	8.897	volume *S* box	S_A [psu]	30	average salinity of Arctic Ocean
V_{IP} [10^{16} m^3]	22.02	volume *IP* box	α [kg/(m^3·°C)]	0.12	thermal expansion coefficient
V_B [10^{16} m^3]	86.49	volume *B* box	β [kg/(m^3·psu)]	0.79	haline contraction coefficient
A_N [10^{12} m^2]	8.1525	surface area *N* box	λ [10^6 m^6/(kg·s)]	27.9	AMOC density difference coefficient
A_T [10^{12} m^2]	77.77	surface area *T* box	γ	0.39	proportion of AMOC entering CWP
A_S [10^{12} m^2]	88.97	surface area *S* box	η [Sv]	74.492	*S*-*B* boxes mixing parameter
A_{IP} [10^{12} m^2]	220.2	surface area *IP* box	K_N [Sv]	5.456	northern subtropical gyre coefficient
C_N	0.07	hosing fraction *N* box	K_S [Sv]	5.447	southern subtropical gyre coefficient
C_T	0.752	hosing fraction *T* box	K_{IP} [Sv]	96.817	Indo-Pacific gyre coefficient
C_S	-0.257	hosing fraction *S* box	μ^a [10^{-6} m/s]	5.0	atmosphere-ocean heat exchange rate
C_{IP}	-0.565	hosing fraction *IP* box	T_N^a [°C]	-3.6924	atmospheric temperature *N* box
F_N [Sv]	0.384	freshwater flux into *N* box	T_T^a [°C]	18.0611	atmospheric temperature *T* box
F_T [Sv]	-0.723	freshwater flux into *T* box	T_S^a [°C]	2.0201	atmospheric temperature *S* box
F_S [Sv]	1.078	freshwater flux into *S* box	T_{IP}^a [°C]	18.0611	atmospheric temperature *IP* box

Table D1. BST parameter values.

q_0[Sv]	ν_{10}	ν_{15}	ν_{20}
1.0	0.02817	0.04135	0.05400
4.0	0.03651	0.05439	0.07209
6.5	0.04847	0.07376	0.10002
9.0	0.07209	0.11459	0.16326
12.0	0.17354	0.34117	0.67672
q_0[Sv]	ν_2	ν_3	ν_4
14.25	0.08406	0.146021	0.23174

https://doi.org/10.5194/egusphere-2025-6565
Preprint. Discussion started: 30 January 2026

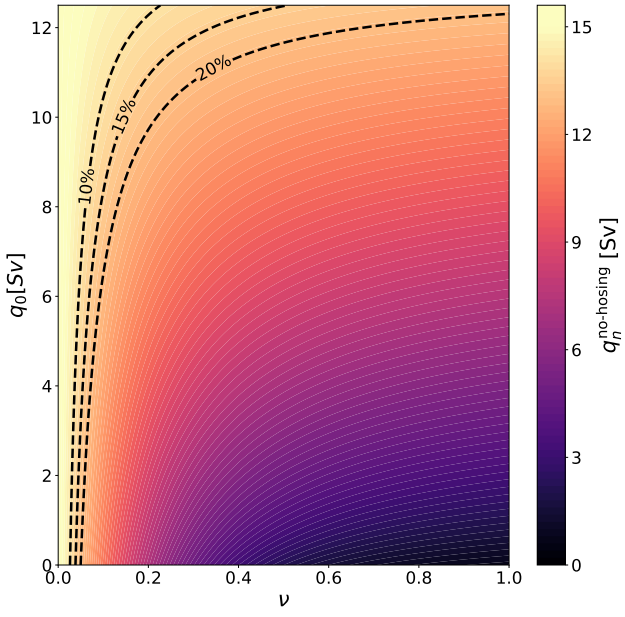

Figure D1. The equilibrium AMOC strengths under no-hosing ($F_H = 0$ Sv) for several values of (v, q_0), where the dashed level curves indicate parameter values for which a closure increases the equilibrium AMOC strength by either 10%, 15% or 20%.

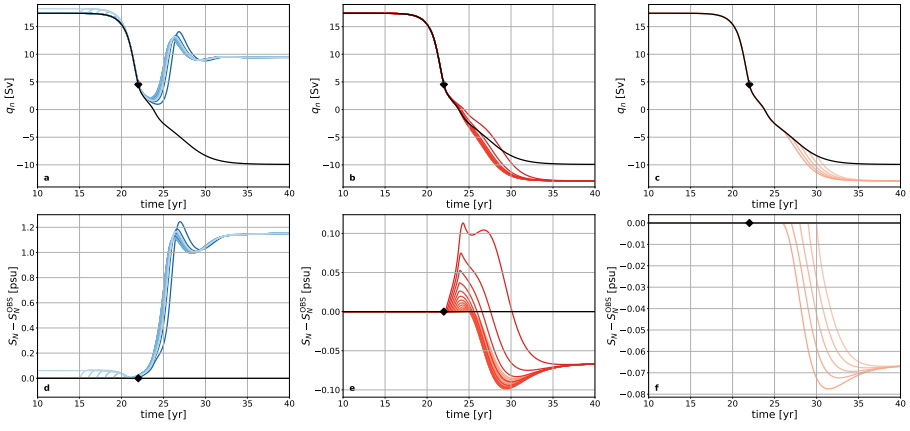

Figure E1. The trajectories shown in Figure 8a and Figure 8b are split into **a**, **b** and **c**, and **d**, **e** and **f** respectively, using the same color scheme. The left plots show trajectories where a closure occurs before the latest preventive closure time t_c^f, the middle plots show trajectories where a closure occurs after t_c^f but before an open Strait starts salinifying the North Atlantic ($\Phi_b > 0$ psu/yr), and the right plots show trajectories where a closure occurs after Φ_b has turned positive. To each the OBS reference trajectory (black, solid) is added, together with the diamond indicating time t_c^f.

https://doi.org/10.5194/egusphere-2025-6565
Preprint. Discussion started: 30 January 2026

Author contributions. JS and EV conceived the extended box model. JS performed the analyses and produced the figures. All authors helped with interpreting the results and drafting the paper.

Competing interests. The authors declare that there are no competing interests present.

Acknowledgements. The authors would like to thank Sacha Sinet for his help with setting up the bifurcation analysis. J.S., E.V. and H.A.D. are funded by the European Research Council through ERC-AdG project TAOC (project 101055096).

https://doi.org/10.5194/egusphere-2025-6565
Preprint. Discussion started: 30 January 2026

References

Alkhayuon, H., Ashwin, P., Jackson, L. C., Quinn, C., and Wood, R. A.: Basin bifurcations, oscillatory instability and rate-induced thresholds for Atlantic meridional overturning circulation in a global oceanic box model, Proceedings of the Royal Society A, 475, 20190 051, 2019.

Armstrong McKay, D. I., Staal, A., Abrams, J. F., Winkelmann, R., Sakschewski, B., Loriani, S., Fetzer, I., Cornell, S. E., Rockström, J., and Lenton, T. M.: Exceeding 1.5 C global warming could trigger multiple climate tipping points, Science, 377, eabn7950, 2022.

Ashwin, P., Wieczorek, S., Vitolo, R., and Cox, P.: Tipping points in open systems: bifurcation, noise-induced and rate-dependent examples in the climate system, Philosophical Transactions of the Royal Society A: Mathematical, Physical and Engineering Sciences, 370, 1166–1184, 2012.

Boers, N.: Observation-based early-warning signals for a collapse of the Atlantic Meridional Overturning Circulation, Nature Climate Change, 11, 680–688, 2021.

Bonino, G., Iovino, D., Brodeau, L., and Masina, S.: The bulk parameterizations of turbulent air–sea fluxes in NEMO4: the origin of sea surface temperature differences in a global model study, Geoscientific Model Development, 15, 6873–6889, 2022.

Boot, A. A. and Dijkstra, H. A.: Physics of AMOC multistable regime shifts due to freshwater biases in an EMIC, Earth System Dynamics, 16, 1221–1235, 2025.

Canadell, J. G., Monteiro, P. M., Costa, M. H., Da Cunha, L. C., Cox, P. M., Eliseev, A. V., Henson, S., Ishii, M., Jaccard, S., Koven, C., et al.: Global carbon and other biogeochemical cycles and feedbacks, IPCC AR6 WGI, final government distribution, pp. chapter–5, 2021.

Cessi, P.: A simple box model of stochastically forced thermohaline flow, Journal of physical oceanography, 24, 1911–1920, 1994.

Cessi, P.: Control of Bering Strait transport by the meridional overturning circulation, Journal of Physical Oceanography, 50, 1853–1870, 2020.

Chapman, R., Ashwin, P., Baker, J., and Wood, R.: Quantifying risk of a noise-induced AMOC collapse from northern and tropical Atlantic Ocean variability, Environmental Research Communications, 6, 111 003, 2024.

Cimatoribus, A. A., Drijfhout, S. S., and Dijkstra, H. A.: Meridional overturning circulation: stability and ocean feedbacks in a box model, Climate dynamics, 42, 311–328, 2014.

Dai, A.: Arctic amplification is the main cause of the Atlantic meridional overturning circulation weakening under large CO2 increases, Climate Dynamics, 58, 3243–3259, 2022.

De Boer, A. M. and Nof, D.: The Bering Strait's grip on the northern hemisphere climate, Deep Sea Research Part I: Oceanographic Research Papers, 51, 1347–1366, 2004.

Dijkstra, H. A.: Characterization of the multiple equilibria regime in a global ocean model, Tellus A: Dynamic Meteorology and Oceanography, 59, 695–705, 2007.

Dijkstra, H. A.: The role of conceptual models in climate research, Physica D: Nonlinear Phenomena, 457, 133 984, 2024.

Ditlevsen, P. and Ditlevsen, S.: Warning of a forthcoming collapse of the Atlantic meridional overturning circulation, Nature Communications, 14, 1–12, 2023.

Frajka-Williams, E., Ansorge, I. J., Baehr, J., Bryden, H. L., Chidichimo, M. P., Cunningham, S. A., Danabasoglu, G., Dong, S., Donohue, K. A., Elipot, S., et al.: Atlantic meridional overturning circulation: Observed transport and variability, Frontiers in Marine Science, 6, 260, 2019.

Hasumi, H.: Sensitivity of the global thermohaline circulation to interbasin freshwater transport by the atmosphere and the Bering Strait throughflow, Journal of climate, 15, 2516–2526, 2002.

https://doi.org/10.5194/egusphere-2025-6565
Preprint. Discussion started: 30 January 2026

Hu, A. and Meehl, G. A.: Bering Strait throughflow and the thermohaline circulation, Geophysical Research Letters, 32, 2005.

Hu, A., Meehl, G. A., Han, W., Timmermann, A., Otto-Bliesner, B., Liu, Z., Washington, W. M., Large, W., Abe-Ouchi, A., Kimoto, M., et al.: Role of the Bering Strait on the hysteresis of the ocean conveyor belt circulation and glacial climate stability, Proceedings of the National Academy of Sciences, 109, 6417–6422, 2012.

Hu, A., Meehl, G. A., Han, W., Otto-Bliestner, B., Abe-Ouchi, A., and Rosenbloom, N.: Effects of the Bering Strait closure on AMOC and global climate under different background climates, Progress in Oceanography, 132, 174–196, 2015.

Hu, A., Meehl, G. A., Abe-Ouchi, A., Han, W., Otto-Bliesner, B., He, F., Wu, T., Rosenbloom, N., Strand, W. G., and Edwards, J.: Dichotomy between freshwater and heat flux effects on oceanic conveyor belt stability and global climate, Communications Earth & Environment, 4, 246, 2023.

Inglis, G. N., Bragg, F., Burls, N. J., Cramwinckel, M. J., Evans, D., Foster, G. L., Huber, M., Lunt, D. J., Siler, N., Steinig, S., Tierney, J. E., Wilkinson, R., Anagnostou, E., de Boer, A. M., Dunkley Jones, T., Edgar, K. M., Hollis, C. J., Hutchinson, D. K., and Pancost, R. D.: Global mean surface temperature and climate sensitivity of the early Eocene Climatic Optimum (EECO), Paleocene–Eocene Thermal Maximum (PETM), and latest Paleocene, Climate of the Past, 16, 1953–1968, 2020.

Johns, W. E., Baringer, M. O., Beal, L., Cunningham, S., Kanzow, T., Bryden, H. L., Hirschi, J., Marotzke, J., Meinen, C., Shaw, B., et al.: Continuous, array-based estimates of Atlantic Ocean heat transport at 26.5 N, Journal of Climate, 24, 2429–2449, 2011.

Marotzke, J.: Abrupt climate change and thermohaline circulation: Mechanisms and predictability, Proceedings of the National Academy of Sciences, 97, 1347–1350, 2000.

Rahmstorf, S., Crucifix, M., Ganopolski, A., Goosse, H., Kamenkovich, I., Knutti, R., Lohmann, G., Marsh, R., Mysak, L. A., Wang, Z., et al.: Thermohaline circulation hysteresis: A model intercomparison, Geophysical Research Letters, 32, 2005.

Ritchie, P. D., Alkhayuon, H., Cox, P. M., and Wieczorek, S.: Rate-induced tipping in natural and human systems, Earth System Dynamics, 14, 669–683, 2023.

Sasgen, I., Wouters, B., Gardner, A. S., King, M. D., Tedesco, M., Landerer, F. W., Dahle, C., Save, H., and Fettweis, X.: Return to rapid ice loss in Greenland and record loss in 2019 detected by the GRACE-FO satellites, Communications Earth & Environment, 1, 8, 2020.

Sein, D. V., Mikolajewicz, U., Gröger, M., Fast, I., Cabos, W., Pinto, J. G., Hagemann, S., Semmler, T., Izquierdo, A., and Jacob, D.: Regionally coupled atmosphere-ocean-sea ice-marine biogeochemistry model ROM: 1. Description and validation, Journal of Advances in Modeling Earth Systems, 7, 268–304, 2015.

Shaffer, G. and Bendtsen, J.: Role of the Bering Strait in controlling North Atlantic ocean circulation and climate, Nature, 367, 354–357, 1994.

Smith, R.: The FAMOUS climate model (versions XFXWB and XFHCC): description update to version XDBUA, Geoscientific Model Development, 5, 269–276, 2012.

Smith, R. S., Gregory, J. M., and Osprey, A.: A description of the FAMOUS (version XDBUA) climate model and control run, Geoscientific Model Development, 1, 53–68, 2008.

Soons, J. and Dijkstra, H. A.: A Constructed Closure of the Bering Strait can Prevent an AMOC Tipping, arXiv preprint arXiv:2508.19826, 2025.

Soons, J., Grafke, T., and Dijkstra, H. A.: Optimal transition paths for AMOC collapse and recovery in a stochastic box model, Journal of Physical Oceanography, 54, 2537–2552, 2024.

Soons, J., Grafke, T., van Westen, R. M., and Dijkstra, H. A.: Physics of an AMOC Overshoot in a Box Model, Journal of Physics: Complexity, 2025.

https://doi.org/10.5194/egusphere-2025-6565
Preprint. Discussion started: 30 January 2026

Stommel, H.: Thermohaline convection with two stable regimes of flow, Tellus, 13, 224–230, 1961.

Talley, L. D.: Descriptive physical oceanography: an introduction, Academic press, 2011.

Van Westen, R. M. and Baatsen, M. L.: European temperature extremes under different AMOC scenarios in the community Earth system model, Geophysical Research Letters, 52, e2025GL114 611, 2025.

Van Westen, R. M. and Dijkstra, H. A.: Asymmetry of AMOC hysteresis in a state-of-the-art global climate model, Geophysical Research Letters, 50, e2023GL106 088, 2023.

Van Westen, R. M., Jacques-Dumas, V., Boot, A. A., and Dijkstra, H. A.: The role of sea ice insulation effects on the probability of AMOC transitions, Journal of Climate, 37, 6269–6284, 2024a.

Van Westen, R. M., Kliphuis, M., and Dijkstra, H. A.: Physics-based early warning signal shows that AMOC is on tipping course, Science advances, 10, eadk1189, 2024b.

Van Westen, R. M., Katsman, C. A., and Le Bars, D.: Dynamic and Steric Sea-level Changes due to a Collapsing AMOC in the Community Earth System Model, EGUsphere, 2025, 1–25, 2025a.

Van Westen, R. M., Vanderborght, E., Kliphuis, M., and Dijkstra, H. A.: Physics-Based Indicators for the Onset of an AMOC Collapse Under Climate Change, Journal of Geophysical Research: Oceans, 130, e2025JC022 651, 2025b.

Vanderborght, E., Van Westen, R. M., and Dijkstra, H. A.: Feedback processes causing an amoc collapse in the community earth system model, Journal of Climate, 1, 2025.

Willeit, M. and Ganopolski, A.: Generalized stability landscape of the Atlantic meridional overturning circulation, Earth System Dynamics, 15, 1417–1434, 2024.

Willeit, M., Ganopolski, A., Robinson, A., and Edwards, N. R.: The Earth system model CLIMBER-X v1. 0. Part 1: Climate model description and validation, Geoscientific Model Development Discussions, 2022, 1–69, 2022.

Willeit, M., Ilyina, T., Liu, B., Heinze, C., Perrette, M., Heinemann, M., Dalmonech, D., Brovkin, V., Munhoven, G., Börker, J., et al.: The Earth system model CLIMBER-X v1. 0–Part 2: The global carbon cycle, Geoscientific Model Development, 16, 3501–3534, 2023.

Wood, R. A., Rodríguez, J. M., Smith, R. S., Jackson, L. C., and Hawkins, E.: Observable, low-order dynamical controls on thresholds of the Atlantic meridional overturning circulation, Climate Dynamics, 53, 6815–6834, 2019.

Yang, X. and Cessi, P.: The Bering Strait throughflow component of the global mass, heat and freshwater transport, Journal of Geophysical Research: Oceans, 129, e2024JC021 463, 2024.